Journal of Electronic Materials
https://doi.org/10.1007/s11664-026-12930-x

ORIGINAL RESEARCH ARTICLE

# Electrochemical Copolymerization of Some Pyrimidine-*N*-Glycosides-Doped Poly(3,4-Ethylenedioxythiophene)/Polypyrrole Electrodes for Enhanced Supercapacitor Performance

**Nilüfer Koçyiğit[1,2] · Fatma Demir[3] · Özlem Yağci[4,5] · Melih Beşir Arvas[6] · Nuran Kahriman[3]**

Received: 19 February 2026 / Accepted: 13 May 2026
© The Author(s) 2026

## Abstract

In this study, high-performance composite electrodes based on poly(3,4-ethylenedioxythiophene) (PEDOT) and polypyrrole (PPy) were successfully synthesized via electrochemical copolymerization in the presence of two distinct pyrimidine-*N*-glycosides (compounds **1** and **2**) on pencil graphite electrodes (PGE). The structural and morphological properties of the prepared electrodes were systematically characterized by x-ray diffraction (XRD), Fourier transform infrared (FTIR) spectroscopy, Raman spectroscopy, and scanning electron microscopy/energy-dispersive spectroscopy (SEM-EDS) analyses, confirming uniform dopant integration and enhanced crystallinity, especially in PEDOT/PPy/(2)/PGE. Electrochemical evaluations were carried out using cyclic voltammetry (CV), electrochemical impedance spectroscopy (EIS), and galvanostatic charge–discharge (GCD) techniques in a PVA/$H_2$1$SO_4$ gel electrolyte. The PEDOT/PPy/(2)/PGE electrode demonstrated the highest electrochemical performance, achieving remarkable specific capacitance of 195.2 F/g, energy density of 45.8 Wh/kg, and power density of 77.4 W/kg. In a symmetric two-electrode configuration, the PEDOT/PPy/(2)/PGE//PEDOT/PPy/(2)/PGE supercapacitor retained specific capacitance of 61.8 F/g at 5 mV/s, and maintained stable energy storage up to 3.7 Wh/kg. The superior capacitive behavior is attributed to the synergistic interaction between the conducting polymer backbone and the pyrimidine-*N*-glycoside dopant, leading to improved electron/ion transport, enlarged surface area, and optimized microstructure. These results suggest that the pyrimidine-*N*-glycoside-functionalized conducting polymer composites, in particular with compound **2**, hold substantial promise for the development of next-generation electrochemical energy storage devices.

**Keywords** PEDOT · PPy · pyrimidine-*N*-glycoside · electropolymerization · supercapacitor

## Introduction

The demand for energy and the need for energy conservation have increased progressively across the globe as a result of the evolving requirements of modern societies. Fossil fuels have adverse effects, including accelerated consumption and environmental pollution resulting from the emission of greenhouse gases. Renewable resources have disadvantages such as dependence on weather conditions in electricity generation, intermittency, low ability to generate electricity, and low energy efficiency.[1–3] Energy storage systems (ESSs) are needed to account for intermittency and to maintain an appropriate balance between energy generation and demand.[4–6] Rechargeable batteries have been proposed as a potential storage system, but they have numerous limitations (e.g., high discharge rate, poor power output, overheating during charge–discharge cycles).[7,8] In contrast to batteries, supercapacitors offer a number of benefits. For this reason,

✉ Melih Beşir Arvas
mbesirarvas@gmail.com

✉ Nuran Kahriman
nuran_yayli@hotmail.com

1 Department of Basic Pharmaceutical Sciences, Faculty of Pharmacy, Biruni University, 34015 Istanbul, Turkey

2 Biruni University Advanced Technology and Research Center (B@MER), Biruni University, 34015 Istanbul, Turkey

3 Faculty of Science, Department of Chemistry, Karadeniz Technical University, 61080 Trabzon, Turkey

4 Department of Physics, Yildiz Technical University, Istanbul 34200, Turkey

5 Science and Technology Application and Research Center, Yildiz Technical University, Istanbul 34200, Turkey

6 Faculty of Science, Department of Chemistry, Istanbul University, 34320 Fatih, Istanbul, Turkey

Published online: 02 June 2026

the investigation of supercapacitors (SCs) has become a very active field of study due to their many advantageous properties, including high power density, a wide operating temperature window, low internal resistance, and high efficiency.[9–13] Supercapacitors are categorized into three main groups: (a) electric double-layer capacitors (EDLCs), (b) pseudocapacitors (redox electrochemical capacitors), and (c) hybrid supercapacitors.[14–16] SCs or EDLCs utilize an adsorption process whereby electrolyte ions are absorbed onto the electrode materials, thereby storing electrical charges. The capacitance of the double layer can be characterized using two distinct methods: rectangular cyclic voltammograms and constant-current time-dependent linear potential variation.[17,18] Pseudocapacitors are a specific type of supercapacitor that uses metal oxide or conductive polymer electrodes with materials that have high electrochemical pseudocapacitance, and the charge storage mechanism is faradaic.[19] Hybrid supercapacitors have mechanisms based on both faradaic and non-faradaic processes. They are classified into three categories according to their electrode configuration: asymmetric, composite, and battery type. This configuration combines the advantageous characteristics of pseudocapacitors and EDLCs, thereby facilitating the development of high-energy and high-cycle-life SCs.[14,20–22] The materials selected for the electrode of the supercapacitor and the electrolyte employed therein impact the electrochemical performance of the supercapacitor. It is therefore crucial to choose an appropriate electrode and electrolyte.[14] Carbon-based electrodes, such as graphene, activated carbon, and carbon nanotubes, are frequently used in supercapacitors and many electrochemistry applications.[23–27] Electrochemical polymerization has many advantages over other polymerization processes. These include the need for only a very small amount of monomer for polymerization, the rapid reaction, the ability to prevent side reactions by controlling the applied potential, and the ability to control film thickness and conductivity by changing the applied potential, scan rate, and time.[28,29] Conductive polymers such as polyaniline (PANI), poly(3,4-ethylenedioxythiophene) (PEDOT), and polypyrrole (PPy) offer significant advantages due to their properties such as improved electrical conductivity, good adsorption onto surface electrodes, and mechanical durability.[30,31] The surface morphology and charge properties of poly(3,4-ethylenedioxythiophene) (PEDOT) can be easily modified by using different additives during the synthesis process. This has led to the popular application of PEDOT in a wide range of electrochemical applications.[32]

The recent focus in research on pseudocapacitive electrodes has been on developing conducting polymer-based systems. Conducting polymers such as PEDOT and PPy are especially interesting due to the reversible doping–dedoping process they undergo, which allows for the rapid and efficient charging of the electrode via faradaic reaction. However, although the characteristics of these polymers allow for excellent potential as supercapacitor electrodes, there are several limitations associated with the electrode's performance. These include structural organization, surface morphology, and the accessibility of electroactive sites. One method to overcome some of these issues is to create hybrid electrode configurations by incorporating conducting polymers with other functional additives or secondary components. Hybridizing the two material types has demonstrated enhanced electrical conductivity, improved ion diffusion pathways, and increased wetting of the electrode's surface area, resulting in significantly improved electrochemical performance. Specifically, the addition of heteroatomic structural units (i.e., nitrogen-, oxygen-containing functional groups) enables modification of the electronic structure of the electrode allowing for easier charge transfer and additional redox-active sites. Recently, researchers have developed molecular-level design approaches to engineer the electrochemical performance of pseudocapacitive systems. Incorporating functional organic molecules into a matrix of a conducting polymer will influence the interaction of individual molecules within the matrix, improve the electrolyte/electrode interface, and facilitate faster ion transport. While significant advancements have occurred using various functional doped-conducting polymer systems, no investigation has been conducted to evaluate the effectiveness of pyrimidine-*N*-glycoside-based doped conductive polymer systems. As a result, this study introduces a new class of heteroatom-rich pyrimidine-*N*-glycoside additives into PEDOT/PPY matrices to improve charge transfer, ion transport, and the overall electrochemical performance of these systems.

Pyrimidine-*N*-glycosides are a class of glycoconjugates that combine a pyrimidine core with a sugar moiety via a glycosidic nitrogen bond, resulting in molecules that are rich in heteroatoms and stereochemical complexity. Biologically, these glycoconjugates have shown antiproliferative, enzyme inhibitory, antioxidant, and antimicrobial activity. They also have potential as biologically active additives, agrochemicals, and molecular probes for nucleic acid detection. Their modular synthesis makes them attractive scaffolds for medicinal chemistry campaigns and for incorporation into multifunctional materials where heteroatom richness and hydrophilicity are advantageous.[33,34] While the application of pyrimidine in supercapacitor electrodes has been investigated to a limited extent, no prior reports have been identified on the use of *N*-glycosides for such purposes.[35,36] This study represents the first demonstration of employing pyrimidine-*N*-glycoside hybrid compounds as active components in supercapacitors. The combination of these two heteroatom-rich structures introduces multiple nitrogen and oxygen functionalities, which can enhance both electrical double-layer

capacitance through improved surface wettability and pseudocapacitance via redox-active sites. The high heteroatom content is expected to facilitate faradaic charge transfer processes, improve electrolyte interaction, and potentially yield superior electrochemical performance compared to conventional carbon-based electrodes.

The lack of supercapacitor applications related to pyrimidine-*N*-glycoside hybrids in the literature and the preparation of new composite electrodes using these hybrid compounds in this study highlight the originality of our study. In this way, we will contribute to the literature by demonstrating the applicability of these compounds in supercapacitors.

In this study, high-performance composite electrode materials for supercapacitors were synthesized by electrochemical polymerization. The electrochemical properties of PEDOT/PPy/(1)- and PEDOT/PPy/(2)-doped pencil graphite electrode (PGE) composite electrodes synthesized utilizing three-electrode and two-electrode systems were characterized by cyclic voltammetry (CV), galvanostatic charge–discharge (GCD), and electrochemical impedance spectroscopy (EIS) methods. Fourier transform infrared (FTIR) spectroscopy, x-ray diffraction (XRD) microscopy, and scanning electron microscopy (SEM) were used to characterize the structure and morphology of the electrodes for supercapacitor application. The PEDOT/PPy-based composite electrodes doped with pyrimidine-*N*-glycosides (1) and (2) were electrochemically synthesized and comprehensively characterized. The PEDOT/PPy/(2)/PGE electrode exhibited outstanding electrochemical performance, achieving specific capacitance of 195.2 F/g, energy density of 45.8 / kg, and power density of 77.4 W/kg in a three-electrode system. Furthermore, the symmetric supercapacitor device assembled with PEDOT/PPy/(2)/PGE electrodes delivered specific capacitance of 61.8 F/g and sustained energy density of 3.7 Wh/kg under a two-electrode configuration.

## Experimental

### Chemicals

Pyrrole and 3,4-ethylenedioxythiophene (EDOT) used as monomer were obtained from Merck Schuchardt OHG (Hogenbrunn, Germany) and from Sigma-Aldrich, respectively. Acetonitrile ($CH_3CN$) and ethanol ($C_2H_6O$) were purchased from Merck. Lithium perchlorate ($LiClO_4$), poly(vinyl alcohol) (PVA), and sulphuric acid (>95%, $H_2SO_4$) were purchased from Sigma-Aldrich (USA). All chemicals were of analytical grade and were used as received. All of the aqueous solutions were prepared from the Merck Milli-Q Reference Ultrapure Water System.

### Synthesis of Pyrimidine-*N*-glycoside Compounds 1 and 2

Compounds **1** and **2** were synthesized according to procedures in the literature.[33,34,37,38] For compound **1**, a mixture of 2,4,6-trisubstituted pyrimidine (15 mmol, 3.93 g), D-glucose monohydrate (15 mmol, 2.97 g), and glacial acetic acid (15 mmol, 0.85 mL) in DMSO (6 mL) was refluxed at 100°C for 24 h, with reaction progress monitored by thin-layer chromatography (TLC) on silica gel 60 $F_{254}$ plates (Merck) using UV visualization and/or spraying with 10% alcoholic $H_2SO_4$ followed by heating. Upon completion, the reaction mixture was cooled to room temperature and transferred to a separatory funnel, then shaken with chloroform and distilled water. After settling, a solid precipitate formed at the interface. This precipitate was isolated, washed sequentially with chloroform and water to remove unreacted starting materials, and rechecked for purity by TLC. For compound **2**, a mixture of pyrimidine *N*-glycoside (compound **1**, 3 mmol, 1.30 g), acetic anhydride (12 mmol, 1.20 g), and $Na_2CO_3$ (12 mmol, 1.10 g) was stirred at 100°C under reflux for 10–20 min, with reaction progress monitored by TLC on silica gel 60 $F_{254}$ plates (Merck). Upon completion, water was added to quench the reaction, followed by chloroform. The mixture was transferred to a separatory funnel, shaken, and allowed to settle. After phase separation, the organic layer was collected, and the solvent was removed under reduced pressure. The crude product was washed with diethyl ether and dried at room temperature. The structures of compounds **1** and **2** were confirmed by $^1H$ nuclear magnetic resonance (NMR), $^1H$–$^1H$ correlation spectroscopy (COSY), $^{13}C$ attached proton test (APT) NMR, liquid chromatography–tandem mass spectrometry (LC–MS/MS), FTIR, and elemental analysis. The structural formulas of the compounds were given in Fig. 1.

### Preparation of the PVA/$H_2SO_4$ Gelled Electrolyte

For the preparation of the PVA/$H_2SO_4$ gelled electrolyte, 20 ml of 0.5 M $H_2SO_4$ solution was prepared in a beaker, to which 2.0 g of PVA was added and stirred vigorously and continuously at 70°C for 2 h. This PVA solution resulted in the formation of a semi-viscous gel.

### Synthesis of the PEDOT/PPy/(81)/PGE and PEDOT/PPy/(2)/PGE Composites by Electropolymerization

The synthesis of PEDOT and PPy was carried out on a pencil graphite electrode (PGE) (Tombow, USA) with a geometric surface of approximately 0.1 $cm^2$. Before the experiments, 0.1 M pyrrole was freshly distilled, after which 4.5 mL of (0.25 M EDOT, 0.1 M pyrrole, and 0.2 M $LiClO_4$ [as conductive electrolyte] in acetonitrile) was prepared. Separately,

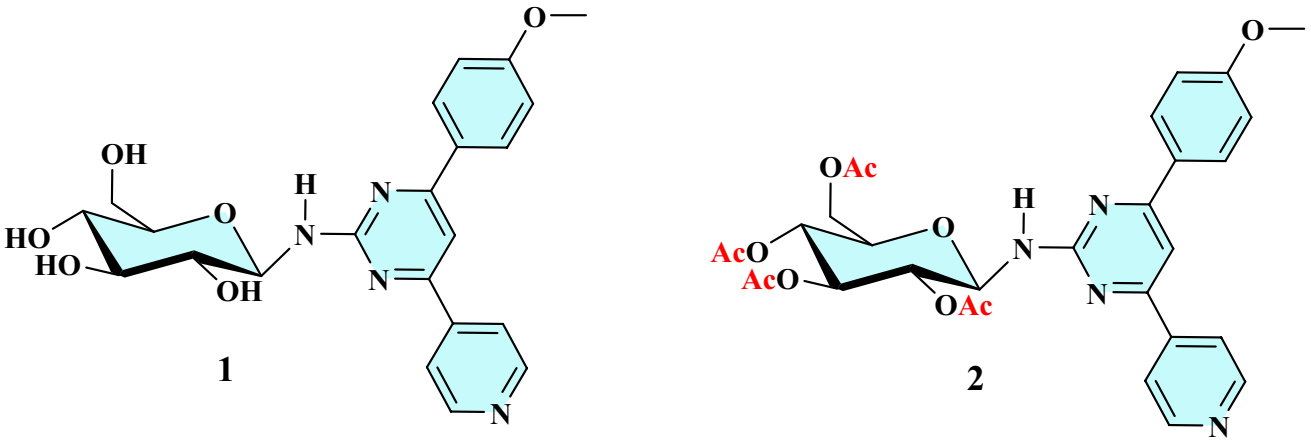


**Fig. 1** Structural formulas of pyrimidine-*N*-glycoside hybrid compounds: compound 1 (free hydroxyl derivative) and compound 2 (acetyl-protected derivative).

the synthesized compound was prepared in 1 mL of ethanol by dissolution in an ultrasonic bath. These two prepared solutions were mixed to obtain a homogeneous solution. A potentiostat/galvanostat (DropSens DRP µSTAT-i 400s, Metrohm, Turkey) was applied for the electrochemical polymerization and cyclic voltammetry measurements of the formed PEDOT and PPy films. The electropolymerization was carried out in a three-electrode system using Ag/AgCl (in 3.0 M KCl solution) as the reference electrode and Pt wire as the auxiliary electrode. All potentials given in this article are with respect to the Ag/AgCl electrode. For the electrochemical polymerization of PEDOT and PPy, 10 cyclic voltammograms were recorded between −1.0 V and 2.0 V at a scan rate of 100 mV $s^{-1}$. Electrochemical measurements for supercapacitor application were performed in 0.5 M $H_2SO_4$/PVA at a scan rate of 50 mV $s^{-1}$.

## Characterization of the PEDOT/PPy/(1)/PGE and PEDOT/PPy/(2)/PGE Composite Electrodes

Electrochemical measurements (CV, EIS, and GCD analysis) were performed using a Gamry 1010E and DropSens DRP µSTAT-i 400s potentiostat/galvanostat (Metrohm, Turkey). To specify the structural parameters of the synthesized electrodes, Raman spectroscopy (Edinburgh Instruments RM5, with a 532-nm laser), XRD (Empyrean MultiCore x-ray diffractometer with Cu-K$\alpha$ radiation, $\lambda = 1.5406$ Å, 45 kV, 40 mA in the $2\theta$ range of 10–90°), and FTIR spectroscopy (PerkinElmer spectrometer in ATR mode) were performed. The morphological properties of the obtained electrodes were investigated using SEM (Zeiss EVO LS 10), coupled with energy-dispersive x-ray (EDX) analysis (EDAX). SEM analysis was performed at magnifications of ×2000, ×20,000, and ×80,000 after coating the electrodes with platinum (Pt) for 120 s.

## Electrochemical Characterization of the PEDOT/PPy/(1)/PGE and PEDOT/PPy/(2)/PGE Composite Electrodes

Electrochemical measurements of the supercapacitor composite electrodes were carried out using CV, GCD, and EIS techniques. The capacitance values of the PEDOT/PPy/(1)/PGE and PEDOT/PPy/(2)/PGE electrodes were calculated from the CV (Eq. 1) and GCD (Eq. 2) measurements according to the following equations:

$$Cs = \frac{\oint_{V1}^{V2} I\,dV}{mv\Delta V}, \tag{1}$$

$$Cs = \frac{I\Delta t}{m\Delta V}. \tag{2}$$

The specific capacitance, $Cs$ (F $g^{-1}$), is calculated from the area $\oint_{V1}^{V2} I\,dV$, which is determined from CV. The potential range, $\Delta V$ (V), is the difference between the initial and final voltage; $m$ (g) is the weight of the active material, $v$ (mV $s^{-1}$) is the scan rate, $I$ (mA) is the current, $\Delta t$ (s) is the discharge time.

Equations 3 and 4 were used to calculate the energy density ($E$) and power density ($P$) values:

$$E = \frac{C \times (\Delta V)^2}{2 \times 4 \times 3.6}, \tag{3}$$

$$P = \frac{3600 \times E}{\Delta t}. \quad (4)$$

The equivalent series resistance (ESR), also known as internal resistance, was calculated using Eq. 5:

$$ESR = IR_{drop}/2I. \quad (5)$$

EIS data were analyzed by fitting the experimental Nyquist plots with an equivalent circuit model. The model consisted of the solution resistance ($R_s$) in series with a parallel combination representing the interfacial charge-transfer resistance and capacitive response, together with a Warburg diffusion element ($W$) to account for ion transport at low frequencies. From this fitting procedure, the electrochemical parameters $R_s$, $R_{ct}$, $C_{dl}$, and $W$ were obtained and used for the comparative evaluation of the electrode and device performance.

## Calculation of Electrochemical Parameters for Symmetric Supercapacitor Device

The electrochemical performance of the symmetric two-electrode supercapacitor device was evaluated using galvanostatic charge–discharge (GCD) measurements. The specific capacitance ($Cs$) of the device was calculated according to Eq. 6:

$$Cs = 2I\ .\Delta t/m\ .\Delta V, \quad (6)$$

where $I$ (A) is the applied current, $\Delta t$ (s) is the discharge time, $\Delta V$ (V) is the potential window excluding the IR drop, and m (g) is the mass of active material on a single electrode.

Alternatively, the same expression can be written as

$$Cs = 4\,I\,\Delta t/m_{total}\Delta V,$$

where $m_{\text{total}}$ is the total mass of active materials on both electrodes. These two expressions are mathematically equivalent and were used to ensure clarity in data interpretation. The energy density ($E$, Wh kg$^{-1}$) and power density ($P$, W kg$^{-1}$) were calculated using Eqs. 7 and 8, respectively:

$$E = Cs.(\Delta V)^2/2\,x\,3.6, \quad (7)$$

$$P = E \times 3600/\Delta t. \quad (8)$$

All calculations were performed consistently for the symmetric device configuration.

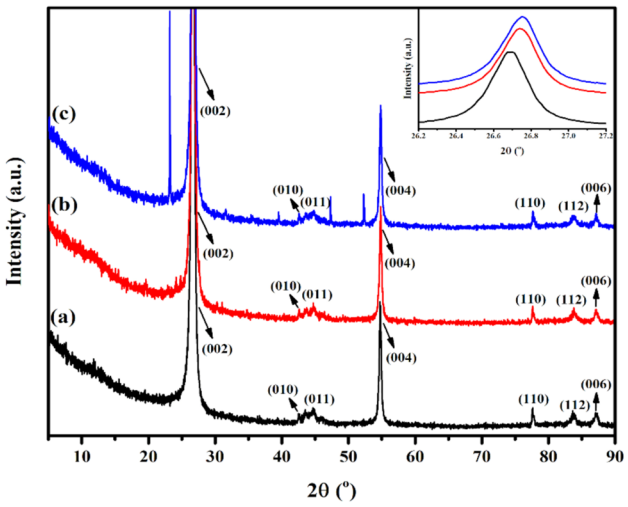


**Fig. 2** XRD patterns of (a) PEDOT/PPy/PGE, (b) PEDOT/PPy/(1)/PGE, and (c) PEDOT/PPy/(2)/PGE electrodes.

## Results and Discussion

### Characterization

Structural characterization of the produced PEDOT/PPy/PGE, PEDOT/PPy/(1)/PGE and PEDOT/PPy/(2)/PGE electrodes was performed by XRD, Raman, and FTIR analyses. Figure 2 shows the XRD patterns of the electrodes. The XRD pattern of the PEDOT/PPy/PGE electrode showed diffraction peaks at $2\theta = 26.69°$, 42.55°, 44.73°, 54.75°, 77.57°, 83.68°, and 87.07° corresponding to the (002), (010), (011), (004), (110), (112), and (006) planes and $d$-spacing values of 3.34, 2.12, 2.02, 1.67, 1.23, 1.15, and 1.11 Å of graphite in the hexagonal $P6_3/mmc$ space group (ICDD card no: 98-005-2230). The main peak of graphite was observed at $2\theta = 26.74°$ and 26.76°, corresponding to $d$-spacing values of 3.33 Å and 3.32 Å in the XRD patterns of the PEDOT/PPy/(1)/PGE and PEDOT/PPy/(2)/PGE electrodes, respectively. The peaks belonging to the dopant were observed in the XRD pattern of the PEDOT/PPy/(2)/PGE electrode. The full width at half maximum (FWHM) values of the main peak of the PEDOT/PPy/PGE, PEDOT/PPy/(1)/PGE, and PEDOT/PPy/(2)/PGE electrodes were 0.12°, 0.18°, and 0.23°, respectively. This result showed that the peaks of the graphite modified with doped PEDOT and PPy electropolymer were broadened and shifted towards the higher angle region, which caused a decrease in the $d$-spacing values. This means a decrease in the inter-chain distance in the $\pi$–$\pi$ stacking direction and indicates stronger interactions between the conjugated backbones with the inclusion of dopants. Thus, the $\pi$–$\pi^*$ electronic transition becomes easier and thus leads to an increase in conductivity.[39,40,41]

The effect of pyrimidine-*N*-glycoside derivatives on the percent crystallinity ratio of the PEDOT/PPy/PGE electrode was calculated using Eq. 9[42]:

$$\text{Percent Crystallinity} = \frac{I_{\text{crystalline}}}{I_{\text{crystalline}} + I_{\text{amorphous}}}. \quad (9)$$

The crystallinity percentages of the PEDOT/PPy/PGE, PEDOT/PPy/(1)/PGE, and PEDOT/PPy/(2)/PGE electrodes were calculated as 53.34%, 49.76%, and 54.89%, respectively (Table I). These results are consistent with the XRD measurements.

The crystallite sizes of the PEDOT/PPy/PGE, PEDOT/PPy/(1)/PGE, and PEDOT/PPy/(2)/PGE electrodes were calculated according to the Debye–Scherrer formula (Eq. 2).[43] The highest-intensity diffraction peak, which corresponds to the (002) plane of graphite, was used in the calculation.

$$D = \frac{K\lambda}{\beta \cos\cos\theta}, \quad (10)$$

where $D$ is the crystallite size, $K$ is the Scherrer constant and its value is 0.94, $\lambda$ is the radiation wavelength and its value is 1.5406 Å, $\beta$ is the full width at half maximum (FWHM) of the diffraction peaks, and $\theta$ is the diffraction angle. The crystallite sizes of PEDOT/PPy/PGE, PEDOT/PPy/(1)/PGE, and PEDOT/PPy/(2)/PGE electrodes were calculated as 66.73, 47.66 and 37.06 nm, respectively (Table I). Peak broadening was greater in doped electrodes. In proportion to this, the crystallite size decreased.

The Raman spectra of the PEDOT/PPy/PGE, PEDOT/PPy/(1)/PGE, and PEDOT/PPy/2)/PGE electrodes are shown in Fig. 3. In the Raman spectrum of the PEDOT/PPy/PGE electrode, two characteristic bands corresponding to the symmetric and asymmetric stretching PEDOT/PPY rings were observed at 1404 and 1602 $cm^{-1}$. In addition, bands corresponding to the C–$N^+$ stretching mode of the polaron radical cation at 1362 $cm^{-1}$ and the C–H bending of the PEDOT/PPy rings at 1004 $cm^{-1}$ were observed.[44] Additionally, bands attributed to $C_\alpha$–$C_{\alpha'}$ stretching, $C_\beta$–$C_{\text{alkyl}}$ stretching, and $C_\alpha$–S–$C_{\alpha'}$ ring deformation of PEDOT were observed at 1110, 950, and 660 $cm^{-1}$, respectively.[45] No new peaks were observed in the Raman spectra of the PEDOT/PPy/(1)/PGE and PEDOT/PPy/(2)/PGE electrodes. However, the intensities and positions of the existing peaks had changed. It was observed that the characteristic stretching modes shifted to the lower wavenumber region due to the strong interaction between the (**1**) and (**2**) pyrimidine-*N*-glycosides and PEDOT/PPy. In addition, it was observed that the peaks in the Raman spectrum of the PEDOT/PPy/(2)/PGE electrode were narrower and had higher intensity. This result, which is consistent with the XRD results, indicates higher crystallinity.

Figure 4a, b, and c show the FTIR spectra of the PEDOT/PPy/PGE, PEDOT/PPy/(1)/PGE, and PEDOT/PPy/(2)/PGE

**Table I** Structural parameters of the peaks corresponding to the (002) plane of the PEDOT/PPy/PGE, PEDOT/PPy/(1)/PGE, and PEDOT/PPy/2)/PGE electrodes

| Electrodes | Peak position $2\theta$ (°) | *d*-spacing (Å) | Percent crystallinity (%) | Crystallite size (nm) |
|---|---|---|---|---|
| PEDOT/PPy/PGE | 26.69 | 3.34 | 53.34 | 66.73 |
| PEDOT/PPy/(1)/PGE | 26.74 | 3.33 | 49.76 | 47.66 |
| PEDOT/PPy/(2)/PGE | 26.76 | 3.32 | 54.89 | 37.06 |

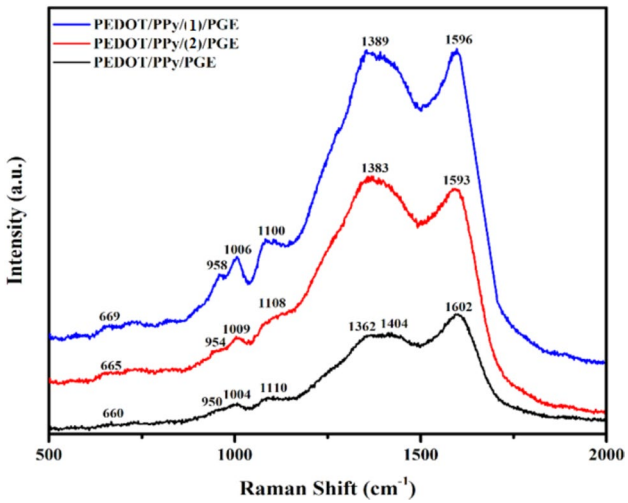


**Fig. 3** Raman spectra of PEDOT/PPy/PGE, PEDOT/PPy/(1)/PGE, and PEDOT/PPy/(2)/PGE electrodes.

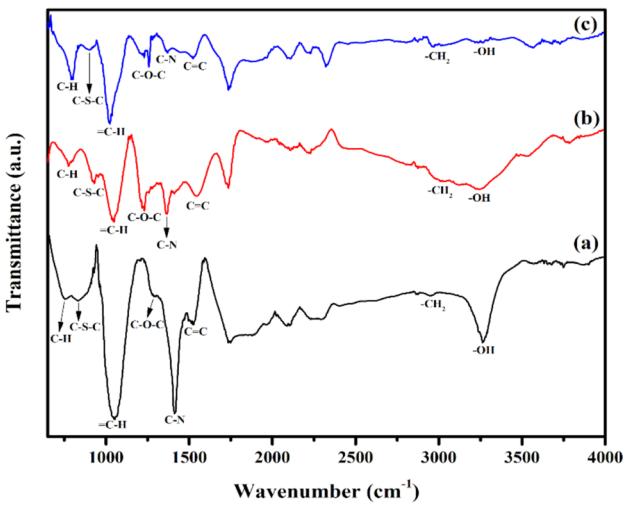


**Fig. 4** FTIR spectra of (a) PEDOT/PPy/PGE, (b) PEDOT/PPy/(1)/PGE, and (c) PEDOT/PPy/(2)/PGE electrodes.

electrodes, respectively. All peaks defining the structure of PEDOT, PPy, and PGE are indicated. In the FTIR spectrum of the PEDOT/PPy/PGE electrode, peaks representing the presence of aliphatic hydrocarbons, $–CH_2$ or $–CH_3$ and –OH stretching band of PGE were observed at 1053 $cm^{-1}$ and 3267 $cm^{-1}$, respectively (Fig. 4a). In addition, peaks were observed at 1523 and 1411 $cm^{-1}$, which were associated with C=C and C–C stretching modes, respectively. Also, peaks were observed at 1291 and 1050 $cm^{-1}$ corresponding to –C–O–C stretching vibration and =C–H out-of-plane vibration, respectively. A peak appeared at 831 $cm^{-1}$ attributed to C–S–C bonding vibration for PEDOT. The peak corresponding to the characteristic C–H vibration associated with the PPy structure was observed at 754 $cm^{-1}$. The characteristic peaks at 831 and 754 $cm^{-1}$ are attributed to the formation of the PEDOT-PPy composite. In the FTIR spectrum, the peaks corresponding to the C=C, C–C, and –C–O–C vibrations were seen to shift to 1544/1367/1227$cm^{-1}$ and 1522/1369/1258 $cm^{-1}$ for the PEDOT/PPy/1)/PGE and PEDOT/PPy/(2)/PGE electrodes, respectively. It was also observed that the intensities of the peaks decreased. The difference in the shifts in the peaks is attributed to the difference in their inter-chain and intra-chain interactions due to the different dopant molecule diameters. The shift of the peak at 1291 $cm^{-1}$ to lower wavenumbers due to doping can be attributed to the elongation of the polymer chain and the increase in conductivity.[46]

SEM analyses were carried out to understand the effect of pyrimidine-*N*-glycoside derivatives on the surface morphology and growth mechanism of the electropolymerized PEDOT and PPy. Figure 5a, b, and c show the SEM surface morphologies and elemental maps of the PEDOT/PPy/PGE, PEDOT/PPy/(1)/PGE, and PEDOT/PPy/(2)/PGE electrodes. Figure 5a shows that a smooth cauliflower-like structure was formed in the SEM images of the PEDOT/PPy/PGE electrode at different magnifications. It was observed that the morphology changed significantly with the doping of pyrimidine-*N*-glycoside derivatives. In the SEM image of the PEDOT/PPy/(1)/PGE electrode, it was observed that the size of the spheres decreased and their shapes became slightly more irregular in some regions (Fig. 5b). In the SEM image of the PEDOT/PPy/(2)/PGE electrode (Fig. 5c), it was observed that the number of spherical particles increased and the particle size decreased relative to the other electrodes. The decrease in particle size increases the surface area. In addition, the morphology of the PEDOT/PPy/(2)/PGE electrode exhibited more common dark and light phases. The dark phases play an important role in transporting electrons and the bright layer plays an important role in transporting ions, and this result can account for the improvement in supercapacitor performance.[47]

In the elemental maps of all three electrodes, the signals of C, N, O, and S were observed, and it was confirmed that they were distributed homogeneously throughout the electrodes. Table II shows the EDS results for the produced electrodes. The EDS and elemental map results confirm that PEDOT and PPy were distributed equally on the PEG surface, which confirms the homogeneous distribution of the elemental content. When the electrodes with dopants were compared with the undoped electrode, it was seen that for (**2**), the dopant had a better interaction with PPy and PEDOT and the elemental distributions were more homogeneous. This situation significantly affects the charge transport and therefore the electrochemical behavior.[48]

## Electrochemical Performance of PEDOT/PPy/(1)/PGE and PEDOT/PPy/(2)/PGE Supercapacitor Electrodes

A mixture of 0.25 M EDOT and 0.1 M pyrrole monomers was prepared in 4.5 mL acetonitrile in the presence of 0.2 M $LiClO_4$. Separately, compound **1** was prepared by dissolving in 1 mL ethanol in an ultrasonic bath, and then these solutions were mixed to prepare a new homogeneous solution. In this solution, a film coating was made on the PGE surface by electropolymerization. Electropolymerization was carried out for compound **1** in different amounts (2.5, 5, 10, 15, and 20 mg) with 10 continuous CV cycles at a scan rate of 100 mV $s^{-1}$ between potentials of −1.0 V and 2.0 V. As a result of this coating, the PEDOT/PPy/(1)/PGE composite electrode was obtained. Compound **2** was prepared by the same process, and the PEDOT/PPy/(2)/PGE composite electrode was obtained. The effect of these modified electrodes on the capacitive performance was investigated, and the supercapacitor electrode performance and application study was carried out in 0.5 M PVA/$H_2SO_4$ (10% w/w) gelled electrolyte solution using three-electrode and two-electrode systems. The electrochemical measurements were executed in 0.5 M $H_2SO_4$/PVA gelled electrolyte at a scan rate of 50 mV $s^{-1}$. The results of the CV, GCD tests, and Nyquist plots (obtained from the electrochemical impedance analysis) for the composite electrodes obtained with different amounts of compound **1** are illustrated in Fig. 6a, b, and c. The specific capacitance values recorded for the PEDOT/PPy/(1)/PGE composite electrodes doped onto PEDOT/PSS using compound **1** at different ratios (2.5, 5, 10, 15, and 20 mg) were 10.4, 15.9, 30.5, 20.3, and 2. F/g at a scan rate of 50 mV/s in the potential range from −0.5 V to +0.8 V and in 0.5 M $H_2SO_4$/PVA electrolyte, respectively. The Nyquist diagrams of the PEDOT/PPy/(1)/PGE composite electrodes doped onto PEDOT/PSS using compound **1** at different ratios (2.5, 5, 10, 15, and 20 mg) are shown in Fig. 6b. The $R_s$, $R_{ct}$, $C_{dl}$, and Warburg impedance values obtained from the Nyquist data are shown in Table III. Accordingly, the PEDOT/PPy/(1)/PGE composite electrode doped using 10 mg of compound **1** had the lowest $R_s$ and $R_{ct}$ and the highest $C_{dl}$ and Warburg impedance values. Figure 6c shows the GCD

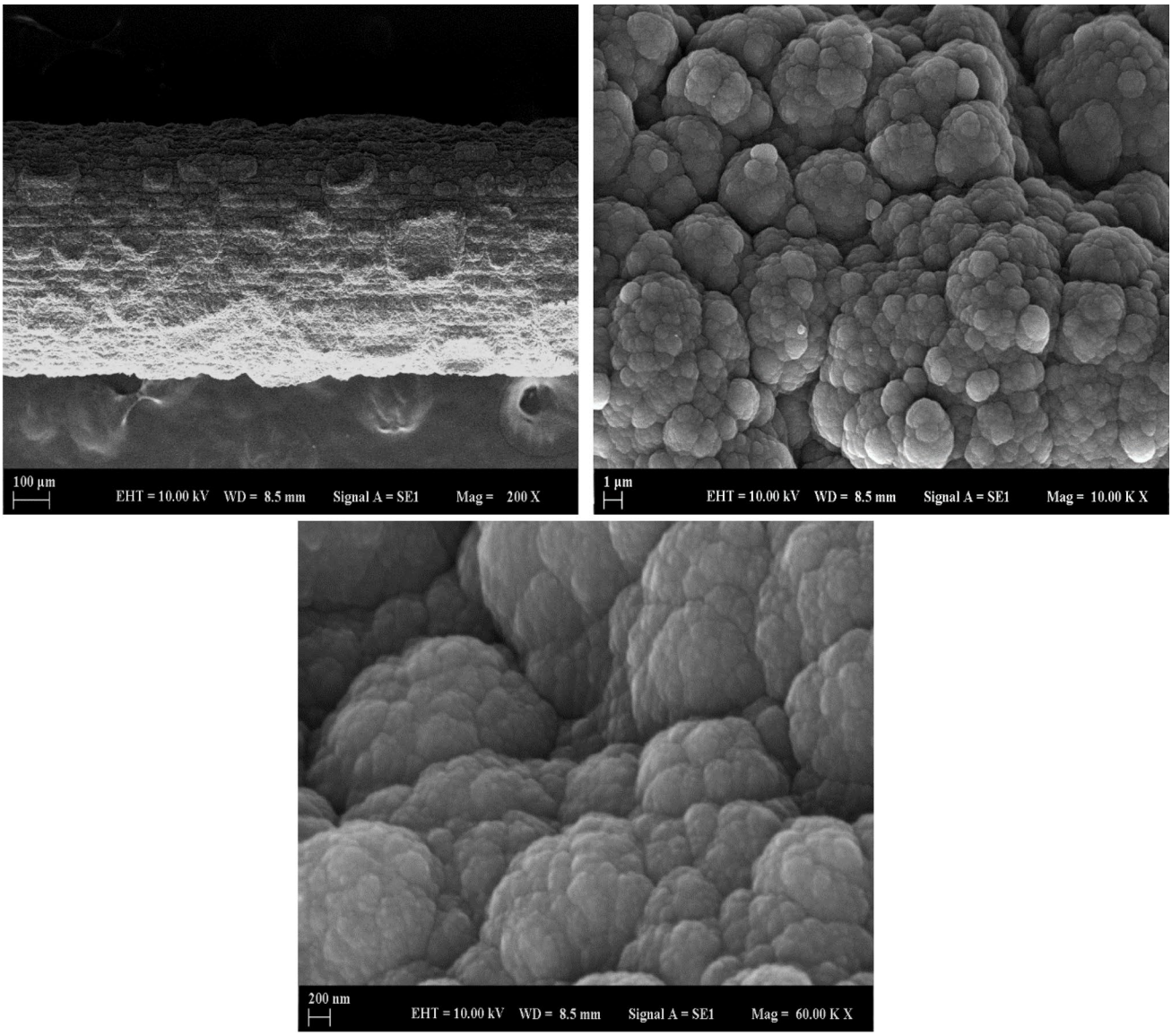


**Fig. 5** SEM images and elemental maps of (a) PEDOT/PPy/PGE, (b) PEDOT/PPy/(1)/PGE, and (c) PEDOT/PPy/(2)/PGE electrodes.

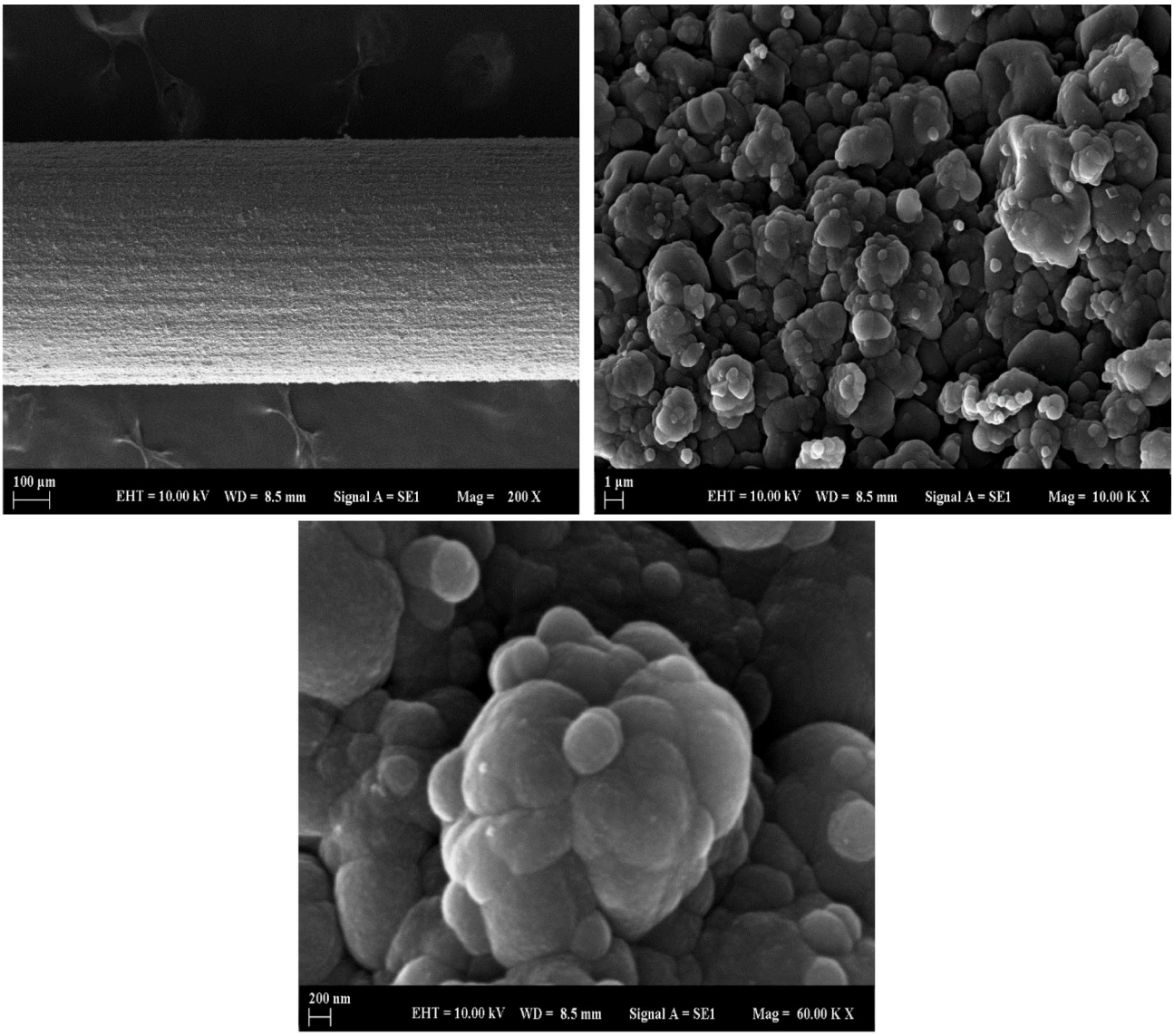


**Fig. 5** (continued)

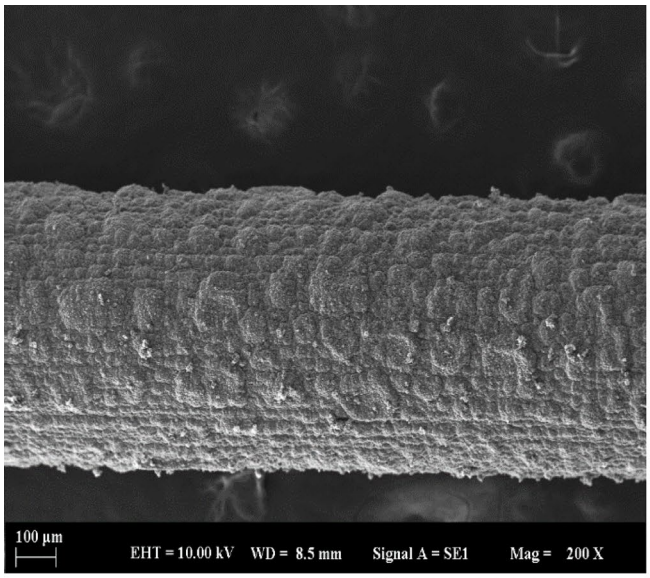


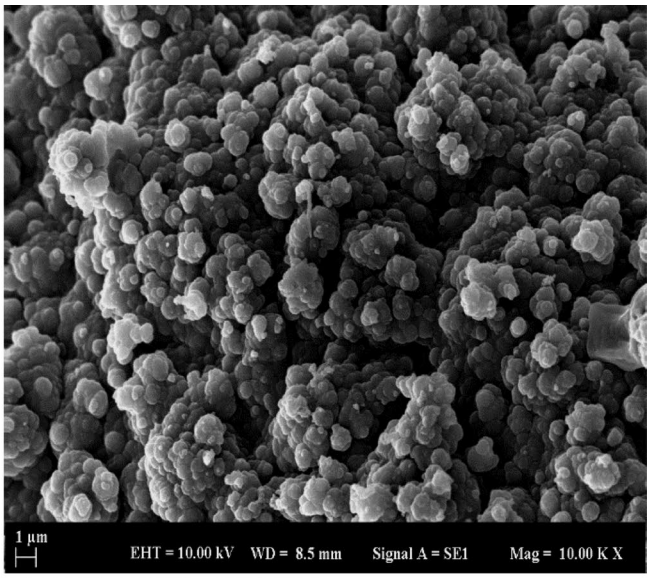


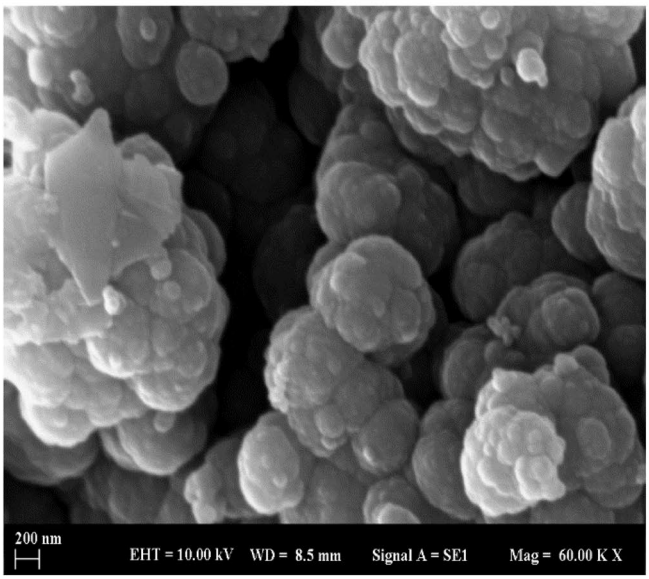


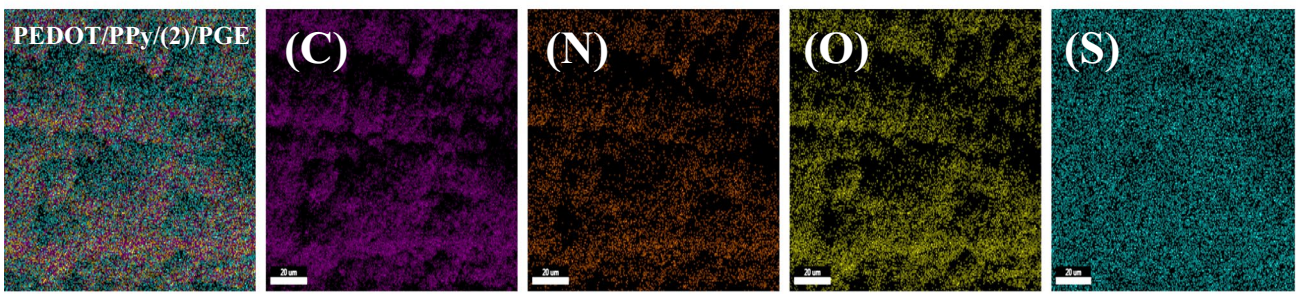


(c)

**Fig. 5** (continued)

**Table II** EDS results for the electrodes

| Element weight (%) | PEDOT/PPy/PGE | PEDOT/PPy/(1)/PGE | PEDOT/PPy/(2)/PGE |
|---|---|---|---|
| C | 45.89 | 60.03 | 48.42 |
| N | 17.68 | 8.74 | 16.76 |
| O | 30.01 | 27.16 | 26.16 |
| S | 6.43 | 4.07 | 8.66 |

curves recorded for the PEDOT/PPy/(1)/PGE composite electrodes doped with different ratios of (**1**) (2.5, 5, 10, 15, and 20 mg) using compound **1** at 500 µA charge–discharge current, in the range of −0.5 V to 0.8 V and in 0.5 M $H_2SO_4$/PVA electrolyte. The specific capacitance values obtained for the PEDOT/PPy/(1)/PGE composite electrodes were 7.0, 9.9, 23.7, 15.1, and 4.3 F/g.

The optimal amount was found to be 10 mg for the electrodes prepared with different amounts of compound **1** using electropolymerization. In the following procedure, electrodes were prepared in 0.5 M PVA/$H_2SO_4$ (10% w/w) gelled electrolyte solution at a scan rate of 100 mV $s^{-1}$ between the potentials of −1.0 V and 2.0 V in 1, 5, 10, 20, and 30 cycles utilizing 10 mg of compound **1**. Electrochemical measurements were carried out in 0.5 M $H_2SO_4$/PVA gel electrolyte at a scan rate of 50 mV $s^{-1}$. The results of the CV, GCD tests, and Nyquist plots (obtained from EIS analysis) for the composite electrodes obtained with different numbers of cycles for compound **1** are shown in Fig. 7a, b, and c. The specific capacitance values obtained for 10 mg of compound **1** prepared at a scan rate of 50 mV/s in the potential range from −0.5 V to +0.8 V and in 0.5 M $H_2SO_4$/PVA gel electrolyte were 9.1, 16.2, 30.5, 40.5, and 26.2 F/g for 1, 5, 10, 20, and 30 cycles, respectively. The Nyquist diagrams of the PEDOT/PPy/(1)/PGE composite electrodes doped onto PEDOT/PSS using compound **1** at different cycles (1, 5, 10, 20, and 30 mg) are shown in Fig. 7b. The $R_s$, $R_{ct}$, $C_{dl}$, and Warburg impedance values obtained from the Nyquist data are shown in Table IV. Figure 7c shows the GCD curves for the PEDOT/PPy/(1)/PGE electrode prepared for 1, 5, 10, 20, and 30 cycles recorded at 500 µA charge–discharge current, in the range of −0.5 V to 0.8 V, and in 0.5 M $H_2SO_4$/PVA electrolyte. The specific capacitance values obtained for the PEDOT/PPy/(1)/PGE electrodes prepared for 1, 5, 10, 20, and 30 cycles were 5.0, 12.9, 23.7, 41.6, and 23.1 F/g, respectively. The highest capacitance value was obtained with 10 mg of additive and 20 cycles of electropolymerization.

It was prepared by dissolving 10 mg of compound **1** in 4.5 mL (0.25 M EDOT, 0.1 M pyrrole, 0.2 M $LiClO_4$ in acetonitrile) and 1 mL of ethanol in an ultrasonic bath. The specific capacitance values of the prepared PEDOT/PPy/(1)/PGE electrode (the electrode with the optimum number of cycles and amount of additives) obtained at different scan rates (5, 10, 25, 50, 100, 250, and 500 mV $s^{-1}$) in 0.5 M $H_2SO_4$/PVA (Fig. 8) were 97.4 ± 8.6 ± 7.7, 80.9 ± 7.9, 61.8 ± 6.3, 49.2 ± 5.1, 36.5 ± 3.4, 17.9 ± 1.6, and 8.2 ± 0.7

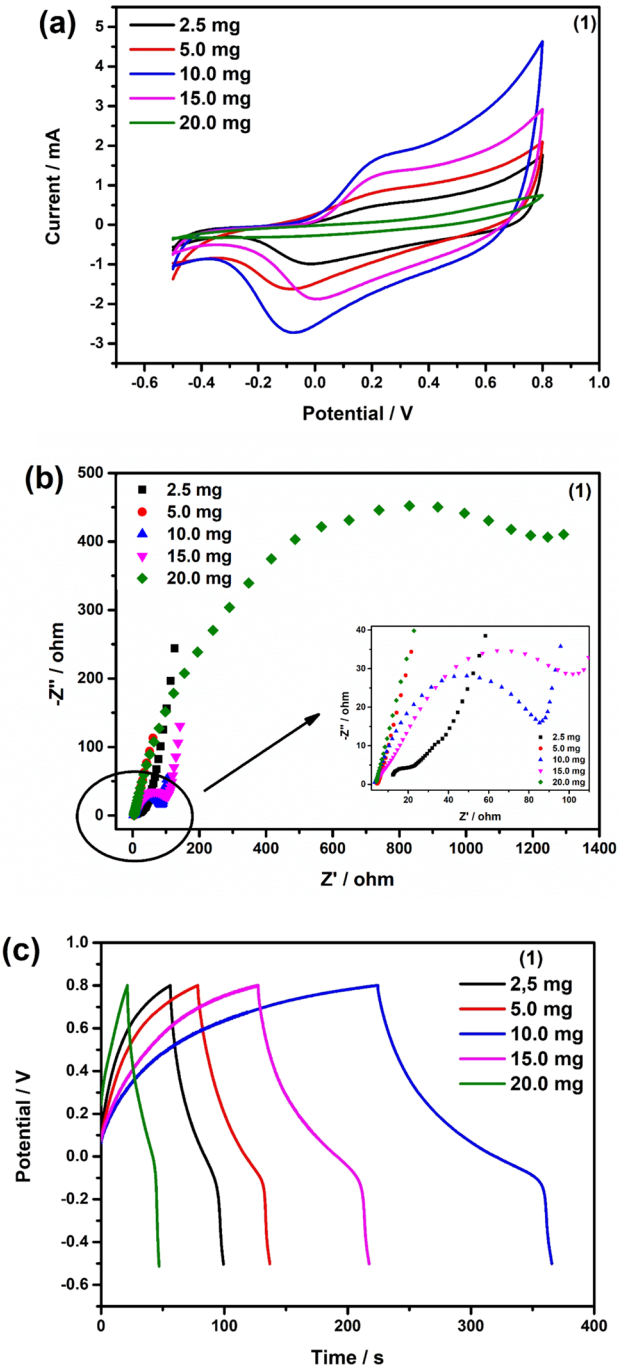


**Fig. 6** Effect of different amounts (2.5, 5, 10, 15, and 20 mg) of compound **1** on the performance of the PEDOT/PPy/(1)/PGE composite electrode in 0.5 M $H_2SO_4$ PVA/$H_2SO_4$ (10% w/w): (a) cyclic voltammograms at 50 mV $s^{-1}$, (b) EIS Nyquist curves, (c) GCD curves at 500 µA.

**Table III** Electrochemical impedance parameters ($R_s$, $R_{ct}$, $C_{dl}$, $W$) of the PEDOT/PPy/(1)/PGE composite electrodes prepared with different amounts (2.5–20 mg) of compound **1**

| Amount of (1) (mg) | $R_s$ (Ω) | $C_{dl}$ (F) | $R_{ct}$ (Ω) | $W$ (Ω $s^{-1/2}$) |
|---|---|---|---|---|
| 2.5 | 12.372 | 1.3598E−4 | 38.833 | 0.0087956 |
| 5.0 | 4.188 | 0.0032419 | 12.738 | 0.010365 |
| 10.0 | 3.355 | 6.2018E−5 | 75.039 | 0.025242 |
| 15.0 | 5.157 | 4.3034E−5 | 89.702 | 0.011615 |
| 20.0 | 6.314 | 3.6044E−5 | 830.202 | 0.0017872 |

F/g, respectively. In addition, the energy density $E$ (Wh/kg) values obtained at different scan rates (5, 10, 25, 50, 100, 250, and 500 mV $s^{-1}$) were 30.4, 25.2, 19.3, 15.3, 11.4, 5.6, and 2.5 Wh/kg, respectively. The specific capacitance values of the PEDOT/PPy/(1)/PGE electrode (the electrode with the optimum number of cycles and doping amount) obtained at different currents (250, 500, 750, 1000, 1500, and 2000 µA) were 86.8 ± 8.9, 74.6 ± 7.3, 60.7 ± 5.8, 48.5 ± 4.9, 34.1 ± 3.2, and 26.8 ± 2.5 F/g, respectively. From the GCD curves (Fig. 9), the energy density values calculated with Eq. 3 were 20.4, 17.5, 14.2, 11.4, 8.0, and 6.3 Wh/kg, respectively. The power density values calculated with Eq. 4 were 70.7, 141.3, 212.0, 282.6, 423.9, and 565.2 W/kg, respectively.

Monomers (0.25 M EDOT and 0.1 M pyrrole) were prepared in 4.5 mL acetonitrile in the presence of 0.2 M $LiClO_4$. Separately, compound **2** was prepared by dissolving it in 1 mL ethanol in an ultrasonic bath. These two solutions were then mixed to produce a new homogeneous solution. The polymers in this solution were coated on the PGE surface in the form of a film by electropolymerization. Electropolymerization was performed for compound **2** with different amounts (2.5, 5, 10, 15, and 20 mg) between potentials −1.0 V and 2.0 V with 10 voltammetry cycles at a scan rate of 100 mV $s^{-1}$. As a result of this coating, a PEDOT/PPy/(2)/PGE composite electrode was obtained. The effect of these modified electrodes on the capacitive performance and electrode performance for supercapacitor application was investigated at a scan rate of 50 mV $s^{-1}$ in 0.5 M PVA/$H_2SO_4$ (10% w/w) gel electrolyte solution using a three-electrode system. The results of CV, GCD tests, and Nyquist plots (obtained from EIS analysis) for these electrodes obtained with different amounts of compound **2** are illustrated in Fig. 9a, b, and c. The specific capacitance values recorded for the PEDOT/PPy/(2)/PGE composite electrodes doped onto PEDOT/PSS using compound **2** at different ratios (2.5, 5, 10, 15, and 20 mg) were 5.0, 8.4, 10.2, 12.6, and 10.5 F/g at a scan rate of 50 mV/s in the potential range from −0.5 V to +0.8 V and in 0.5 M $H_2SO_4$/PVA electrolyte, respectively (Fig. 10a). The Nyquist diagrams of PEDOT/PPy/(2)/PGE composite electrodes doped onto PEDOT/PSS

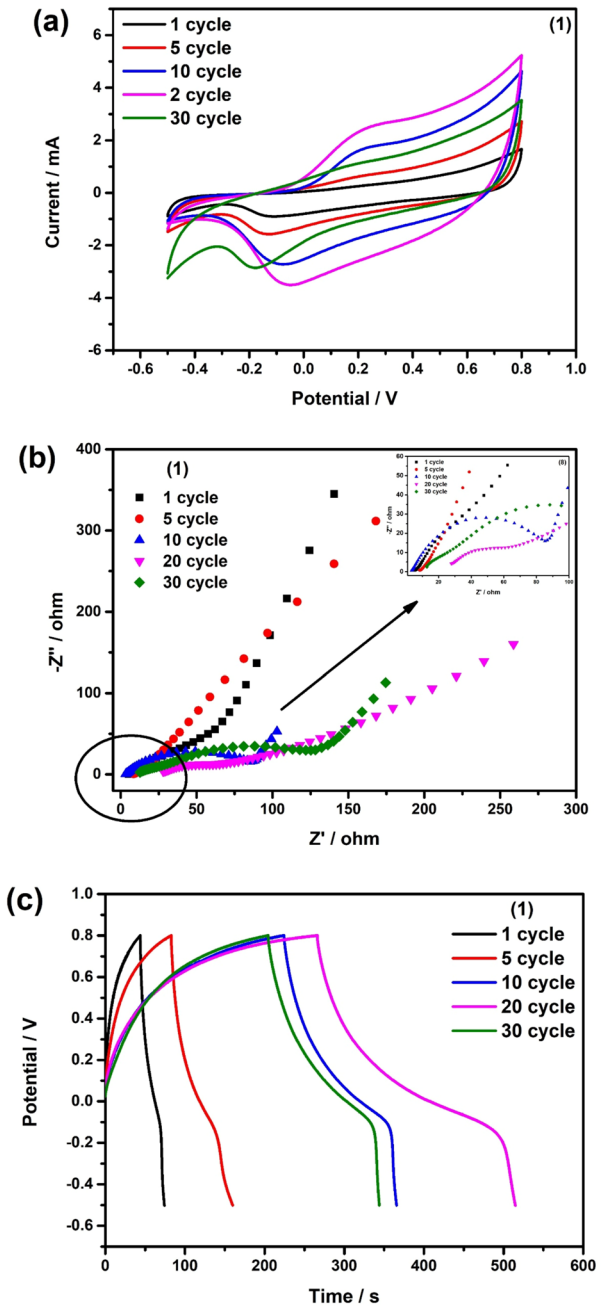


**Fig. 7** Effect of different numbers of cycles (1, 5, 10, 20, and 30) for compound **1** on the performance of the PEDOT/PPy/(1)/PGE composite electrode in 0.5 M $H_2SO_4$ PVA/$H_2SO_4$ (10% w/w): (a) Cyclic voltammograms at 50 mV $s^{-1}$, (b) EIS Nyquist curves, (c) GCD curves at 500 µA.

using compound **2** at different ratios (2.5, 5, 10, 15, and 20 mg) are shown in Fig. 10b. The $R_s$, $R_{ct}$, $C_{dl}$, and Warburg impedance values obtained from the Nyquist data are shown in Table V. Accordingly, the PEDOT/PPy/(2)/PGE composite electrode doped using 15 mg of compound **2** had the lowest $R_s$, $R_{ct}$ and the highest $C_{dl}$ and Warburg impedance values. Figure 10c shows the GCD

**Table IV** Electrochemical impedance parameters ($R_s$, $R_{ct}$, $C_{dl}$, $W$) of the PEDOT/PPy/(1)/PGE composite electrode prepared at different electropolymerization cycles (1–30 cycles)

| Cycle number | $R_s$ (Ω) | $C_{dl}$ (F) | $R_{ct}$ (Ω) | $W$ (Ω $s^{-1/2}$) |
|---|---|---|---|---|
| 1 | 6.392 | 3.063E−4 | 57.543 | 0.0059311 |
| 5 | 8.222 | 0.0010083 | 44.818 | 0.0041923 |
| 10 | 3.355 | 6.2018E−5 | 75.039 | 0.025242 |
| 20 | 27.793 | 3.9296E−6 | 58.566 | 0.00525 |
| 30 | 12.701 | 3.981E−5 | 113.264 | 0.01368 |

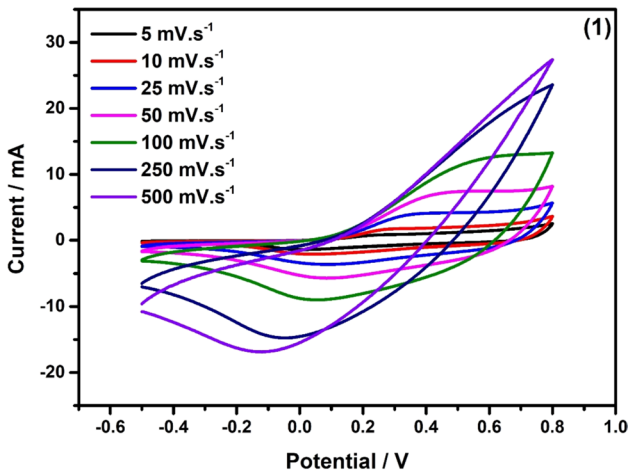


**Fig. 8** Effect of different scan rates (5, 10, 25, 50, 100, 250, and 500 mV $s^{-1}$) for the PEDOT/PPy/(1)/PGE composite electrode (obtained from 20 cycles, 10 mg of compound **1**) in 0.5 M $H_2SO_4$ PVA/$H_2SO_4$ (10% w/w).

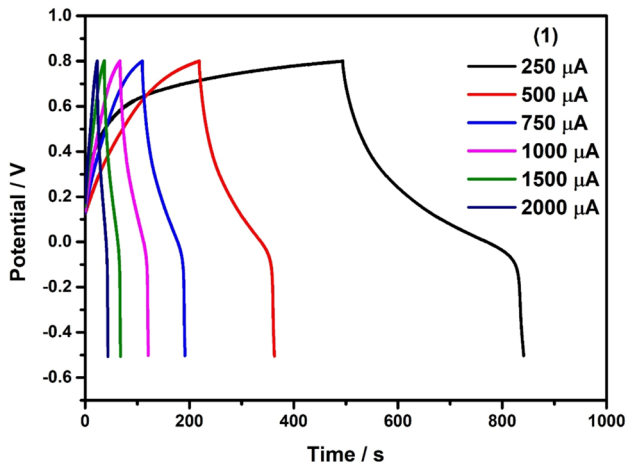


**Fig. 9** Different current values (250, 500, 750, 1000, 1500, and 2000 µA) for the PEDOT/PPy/(1)/PGE composite electrode (obtained from 20 cycles, 10 mg of compound **1**) in 0.5 M $H_2SO_4$ PVA/$H_2SO_4$ (10% w/w).

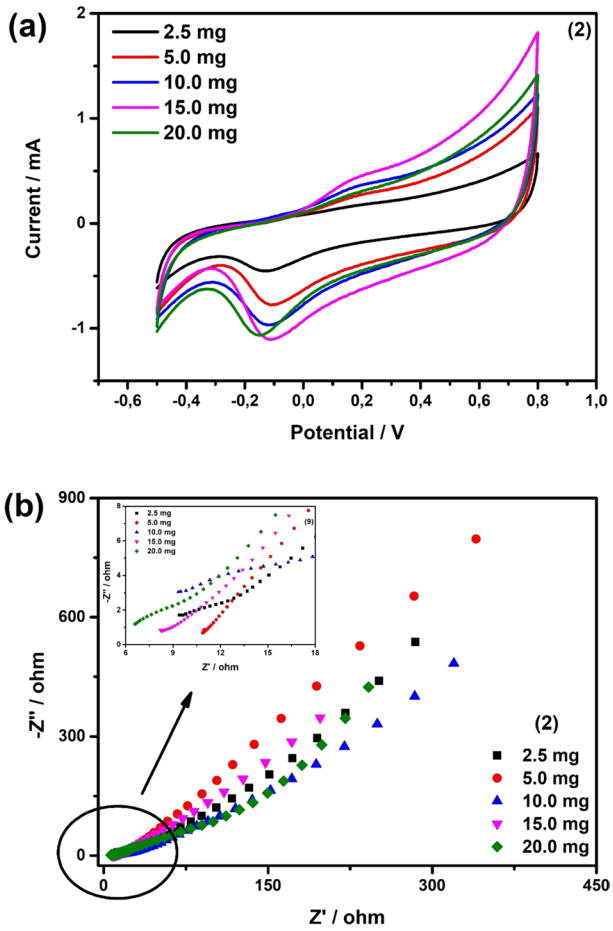


**Fig. 10** Effect of different amounts (2.5, 5, 10, 15, and 20 mg) of compound **2** on the performance of the PEDOT/PPy/(2)/PGE composite electrode in 0.5 M $H_2SO_4$ PVA/$H_2SO_4$ (10% w/w): (a) Cyclic voltammograms at 50 mV $s^{-1}$, (b) EIS Nyquist curves, (c) GCD curves at 500 µA.

curves recorded for the PEDOT/PPy/(2)/PGE composite electrodes doped with different ratios of (**2**) (2.5, 5, 10, 15, and 20 mg) using compound **2** at 500 µA charge–discharge

**Table V** Electrochemical impedance parameters ($R_s$, $R_{ct}$, $C_{dl}$, $W$) of PEDOT/PPy/(2)/PGE composite electrodes prepared with different amounts (2.5–20 mg) of compound **2**

| Amount of (2) (mg) | $R_s$ (Ω) | $C_{dl}$ (F) | $R_{ct}$ (Ω) | $W$ (Ω $s^{-1/2}$) |
|---|---|---|---|---|
| 2.5 | 9.391 | 3.3841E−5 | 14.031 | 0.0030335 |
| 5.0 | 10.879 | 2.2874E−4 | 22.395 | 0.0020078 |
| 10.0 | 9.337 | 2.7033E−6 | 13.929 | 0.0027573 |
| 15.0 | 8.241 | 3.0596E−4 | 19.949 | 0.0042591 |
| 20.0 | 6.597 | 2.2967E−4 | 99.994 | 0.0040611 |

current, in the range of −0.5 V to 0.8 V, and in 0.5 M $H_2SO_4$/PVA electrolyte. The specific capacitance values obtained for the PEDOT/PPy/(2)/PGE composite electrodes were 3.1, 4.8, 6.8, 8.2, and 7.0 F/g.

The optimal amount was found to be 15 mg for the electrodes prepared using different amounts of compound **2** by electropolymerization. In the following procedure, electrodes were prepared in 0.5 M PVA/$H_2SO_4$ (10% w/w) gelled electrolyte solution at a scan rate of 100 mV $s^{-1}$ between the potentials of −1.0 V and 2.0 V in 1, 5, 10, 20, and 30 cycles utilizing 15 mg of compound **2**. Electrochemical measurements were carried out in 0.5 M $H_2SO_4$/PVA gel electrolyte at a scan rate of 50 mV $s^{-1}$. The results of CV and GCD tests and Nyquist plots (obtained from EIS analysis) for the composite electrodes obtained with different numbers of cycles for compound **2** are shown in Fig. 11a, b, and c. The specific capacitance values obtained for 15 mg of compound **2** prepared at a scan rate pf 50 mV/s, in the potential range from −0.5 V to +0.8 V and in 0.5 M $H_2SO_4$/PVA gel electrolyte, were 3.32, 5.94, 10.51, 15.06, 15.17, 29.45, 48.52, and 34.82 F/g for 1, 5, 10, 20 30,40, 50, and 60 cycles, respectively. The Nyquist diagrams of PEDOT/PPy/(2)/PGE composite electrodes doped onto PEDOT/PPy using compound **2** at different cycles (1, 5, 10, 20, 30, 40, 50, and 60 cycles) are shown in Fig. 11b. The $R_s$, $R_{ct}$, $C_{dl}$, and Warburg impedance values obtained from the Nyquist data are shown in Table VI. Figure 11c shows the GCD curves of the PEDOT/PPy/(2)/PGE electrode prepared for 1, 5, 10, 20, 30, 40, 50, and 60 cycles recorded at 500 µA charge–discharge current, in the range of −0.5 V to 0.8 V, and in 0.5 M $H_2SO_4$/PVA electrolyte. The specific capacitance values obtained for the PEDOT/PPy/(2)/PGE electrodes prepared for 1, 5, 10, 20, 30, 40, 50, and 60 cycles were 3.4, 7.0, 11.1, 19.5, 39.3, 81.4, 136.5, 94.7 F/g, respectively. The highest capacitance value was obtained with 15 mg of dopant (**2**) and 50 cycles of electropolymerization.

It was prepared by dissolving 15 mg of compound **2** in 4.5 mL of (0.25 M EDOT, 0.1 M pyrrole, 0.2 M $LiClO_4$ in acetonitrile) and 1 mL of ethanol in an ultrasonic bath. The specific capacitance values of the prepared PEDOT/PPy/(2)/PGE electrode (the electrode with the optimum number of

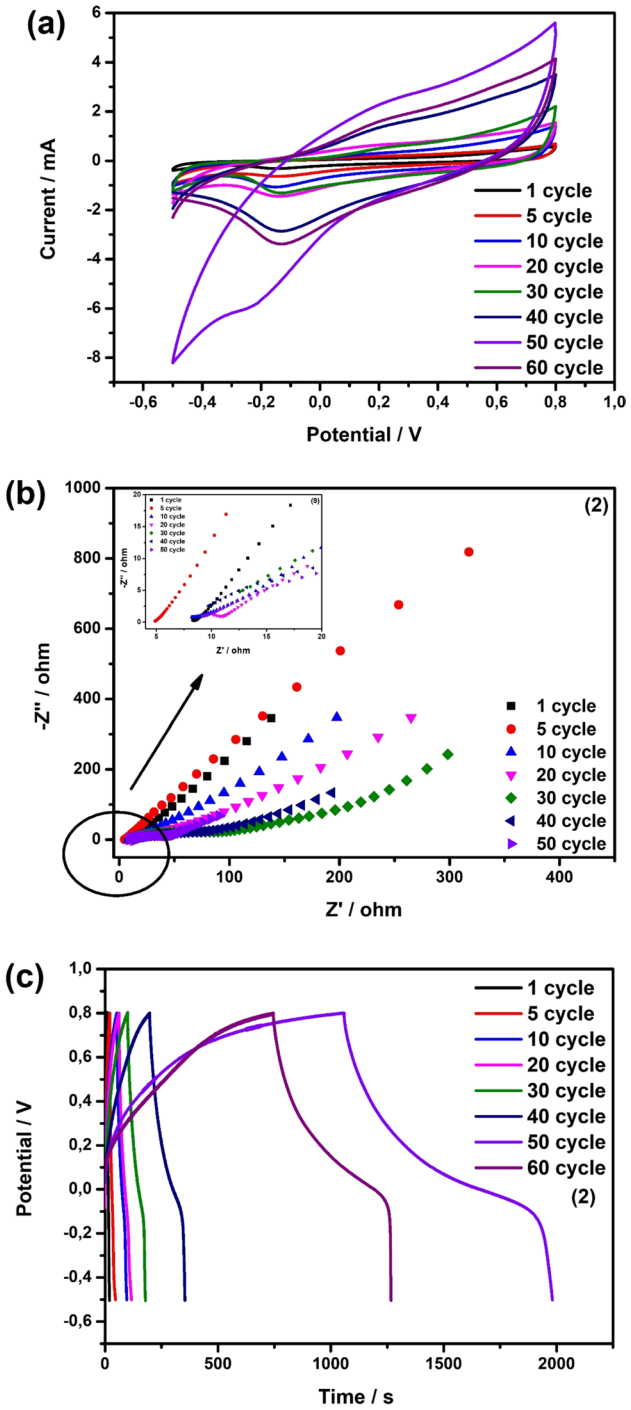


**Fig. 11** Effect of different numbers of cycles (1, 5, 10, 20, and 30) for compound **2** on the performance of the PEDOT/PPy/(2)/PGE composite electrode in 0.5 M $H_2SO_4$ PVA/$H_2SO_4$ (10% w/w): (a) Cyclic voltammograms at 50 mV $s^{-1}$, (b) EIS Nyquist curves, (c) GCD curves at 500 µA.

cycles and amount of additives) obtained at different scan rates (5, 10, 25, 50, 100, 250, and 500 mV $s^{-1}$) in 0.5 M $H_2SO_4$/PVA were 195.6 ± 20.1, 168.0 ± 16.8, 124.7 ± 12.1, 94.1 ± 9.2, 62.0 ± 6.1, 24.2 ± 2.2, and 10.0 ± 0.9 F/g,

**Table VI** Electrochemical impedance parameters ($R_s$, $R_{ct}$, $C_{dl}$, $W$) of PEDOT/PPy/(2)/PGE composite electrodes synthesized with varying cycle numbers (1–60 cycles) using 15 mg of compound **2**

| Cycle number | $R_s$ (Ω) | $C_{dl}$ (F) | $R_{ct}$ (Ω) | $W$ (Ω $s^{-1/2}$) |
|---|---|---|---|---|
| 1 | 8.442 | 0.0012262 | 17.161 | 0.0033895 |
| 5 | 4.875 | 4.8934E−4 | 14.787 | 0.0014457 |
| 10 | 8.241 | 3.0596E−4 | 19.949 | 0.0042591 |
| 20 | 10.972 | 9.973E−5 | 45.393 | 0.0037802 |
| 30 | 12.571 | 1.3147E−6 | 70.831 | 0.0034919 |
| 40 | 9.708 | 8.8711E−6 | 53.684 | 0.0064493 |
| 50 | 9.148 | 5.9673E−5 | 34.623 | 0.018395 |
| 60 | 10.985 | 2.773E−4 | 33.945 | 0.0019162 |

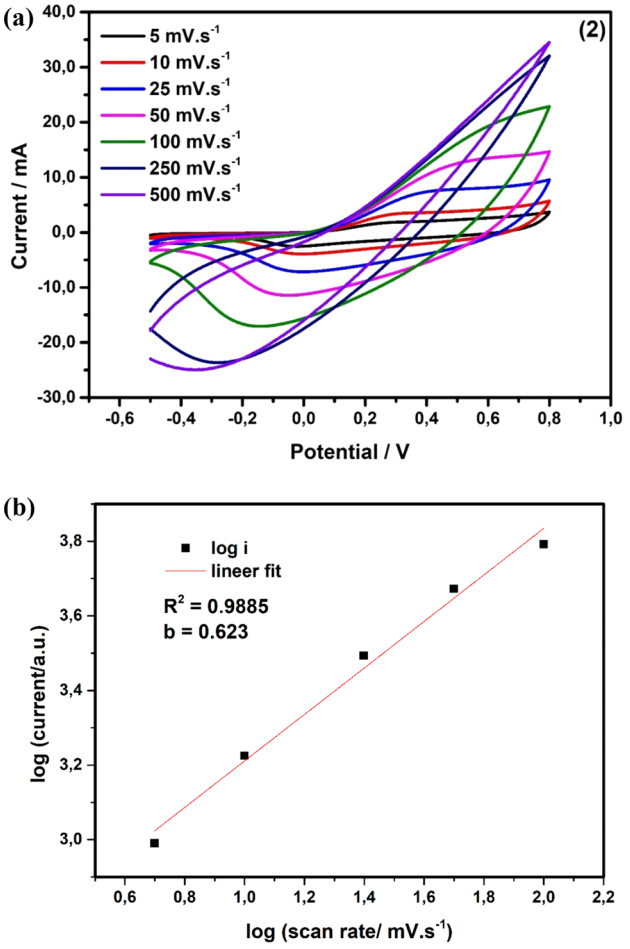


**Fig. 12** (a) Effect of different scan rates (5, 10, 25, 50, 100, 250, and 500 mV $s^{-1}$) for the PEDOT/PPy/(2)/PGE composite electrode (obtained from 50 cycles, 15 mg of compound **2**) in 0.5 M $H_2SO_4$ PVA/$H_2SO_4$ (10% w/w). (b) Apparent *b*-value analysis of the PEDOT/PPy/(2)/PGE composite electrode based on CV-derived response at different scan rates (5–100 mV $s^{-1}$) in PVA/0.5 M $H_2SO_4$ (10% w/w) gel electrolyte.

respectively (Fig. 12). In addition, the energy density *E* (Wh/kg) values obtained at different scan rates (5, 10, 25, 50, 100, 250, and 500 mV $s^{-1}$) were 61.1, 52.5, 38.9, 29.4, 19.3, 7.5, and 3.1 Wh/kg, respectively. The specific capacitance values of the PEDOT/PPy/(2)/PGE electrode (the electrode with the optimum number of cycles and doping amount) obtained at different currents (250, 500, 750, 1000, 1500, and 2000 µA) were 195.2 ± 15.9, 161.5 ± 12.5, 142.3 ± 11.6, 133.3 ± 10.8, 112.6 ± 9.9, and 104.0 ± 9.5 F/g, respectively (Fig. 13). From the GCD curves, the energy and power density values calculated with Eq. 3 were 45.8, 37.9, 33.4, 31.3, 26.4, and 24.4 Wh/kg, respectively. The power density values calculated with Eq. 4 were 77.4, 154.8, 232.1, 309.5, 464.3, and 619.0 W/kg, respectively.

To further clarify the charge-storage kinetics of the PEDOT/PPy/(2)/PGE electrode, an apparent *b*-value analysis was performed using the CV-derived response at different scan rates according to a power-law relationship, i = avb. A plot of log(i) versus log(v) in the low-to-moderate scan rate region (5–100 mV $s^{-1}$) showed good linearity and yielded an apparent *b*-value of 0.623 ($R^2 = 0.9885$). This result indicates that the charge-storage process is governed by a mixed kinetic regime, involving both surface-controlled capacitive contribution and diffusion-limited ion transport. The deviation in *b* from 0.5 toward higher values suggests that the PEDOT/PPy/(2)/PGE electrode benefits from appreciable pseudocapacitive behavior and relatively fast interfacial kinetics. When considered together with the high capacitance values and the comparatively low charge-transfer resistance obtained from EIS, this analysis further supports the conclusion that compound **2** promotes more efficient

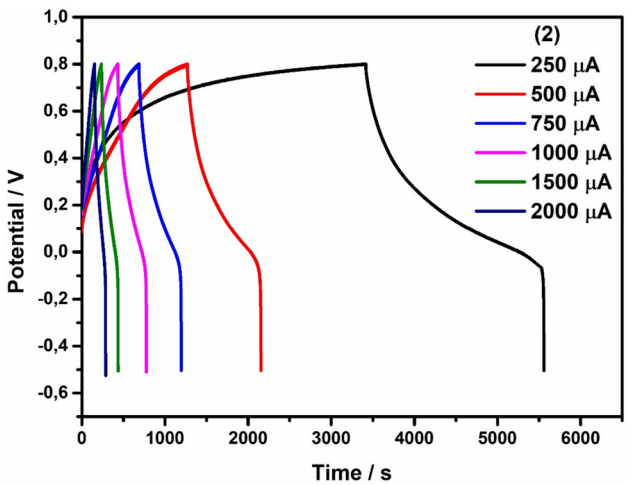


**Fig. 13** Different current values (250, 500, 750, 1000, 1500, and 2000 µA) for the PEDOT/PPy/(2)/PGE composite electrode (obtained from 50 cycles, 15 mg of compound **2**) in 0.5 M $H_2SO_4$ PVA/$H_2SO_4$ (10% w/w).

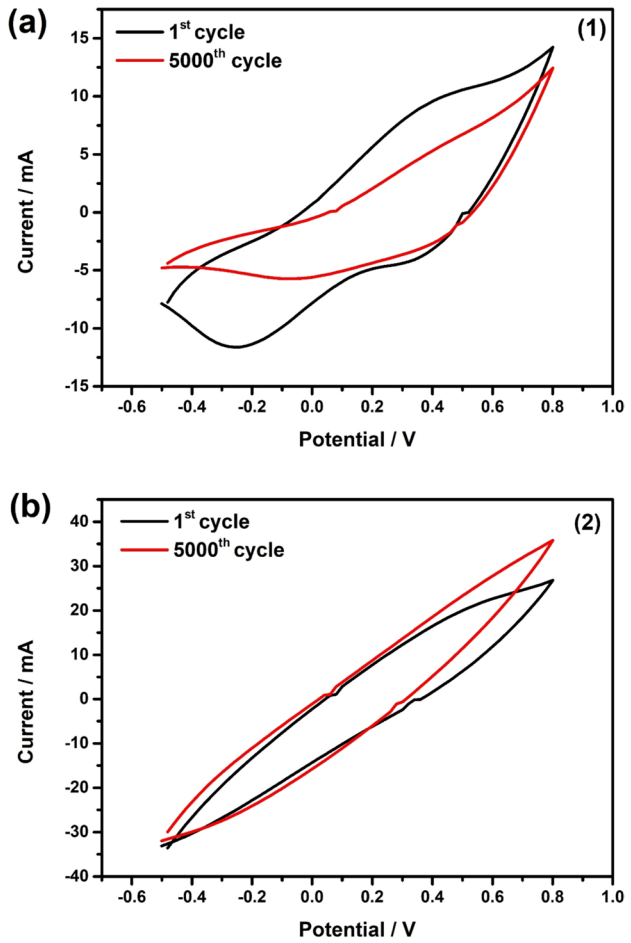


**Fig. 14** (a) Capacitance retention for the PEDOT/PPy/(1)/PGE composite electrode (obtained from 20 cycles, 10 mg of compound **1**) in 0.5 M $H_2SO_4$ PVA/$H_2SO_4$ (10% w/w). (b) Capacitance retention for the PEDOT/PPy/(2)/PGE composite electrode (obtained from 50 cycles, 15 mg of compound **2**) in PVA/0.5 M $H_2SO_4$ (10% w/w).

charge transfer and facilitates ion accessibility within the composite electrode structure.

The capacitance retention of the PEDOT/PPy/(2)/PGE composite electrode was evaluated over 5000 consecutive CV cycles at a scan rate of 100 mV/s in PVA/$H_2SO_4$ (10% w/w) gel electrolyte. As observed in Fig. 14b, the CV curve area after 5000 cycles retained approximately 92.3% of its initial value, indicating excellent electrochemical stability. In comparison, the PEDOT/PPy/(1)/PGE electrode retained about 79.6% of its initial capacitance, suggesting moderate degradation over the same cycling period (Fig. 14a). The superior retention of PEDOT/PPy/(2)/PGE is attributed to its more homogeneous surface morphology, enhanced dopant interaction, and optimized polymer chain organization, which collectively contribute to better structural integrity under prolonged electrochemical stress.

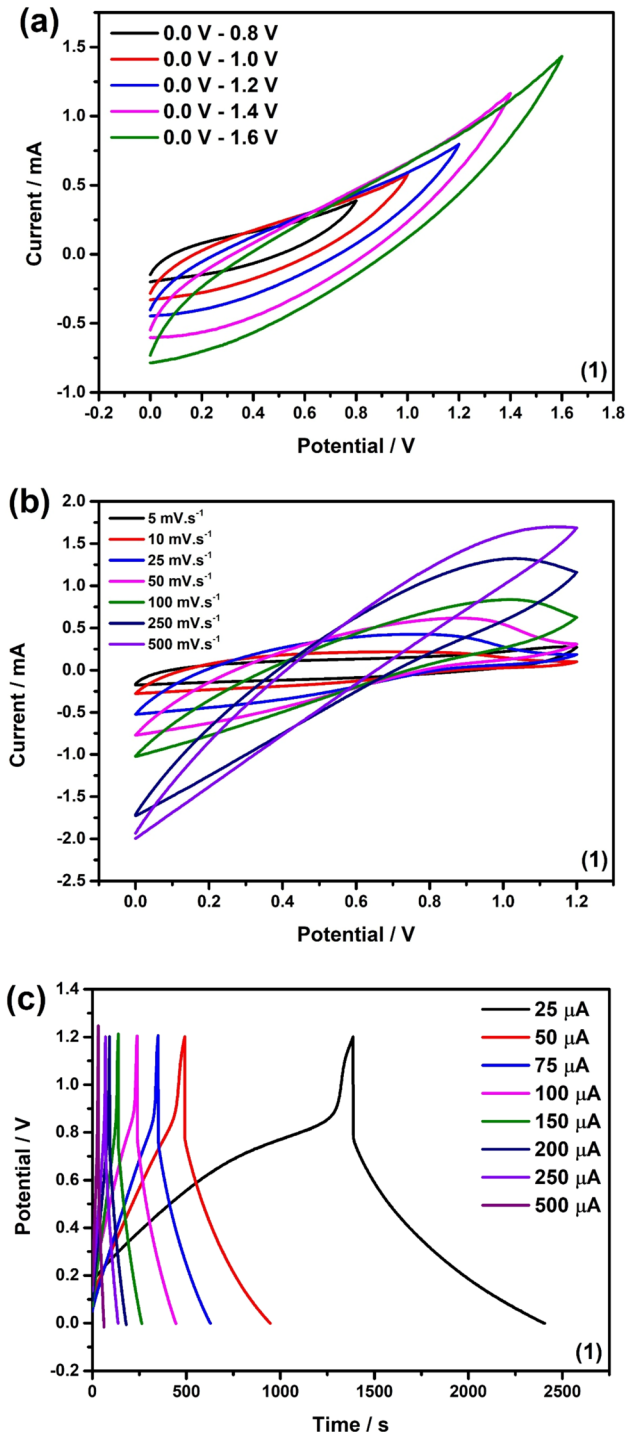


**Fig. 15** PEDOT/PPy/(1)/PGE//PEDOT/PPy/(1)/PGE symmetric supercapacitor in PVA/0.5 M $H_2SO_4$ (10% w/w) electrolyte; (a) CVs recorded in the range of 0.0–0.8 V, 0.0–1.0 V, 0.0–1.2 V, and 0.0 V–1.4 V at a scan rate of 100 mV $s^{-1}$, (b) CVs recorded between 0.0 V and 1.2 V at different scan rates (5, 10, 25, 50, 100, 250, and 500 mV/s); (c) GCD curves recorded between 0.0 V and 1.2 V at different current values; (d) EIS Nyquist curves of before and after long-cycle tests; (e) long-cycle test for 5000 cycles.

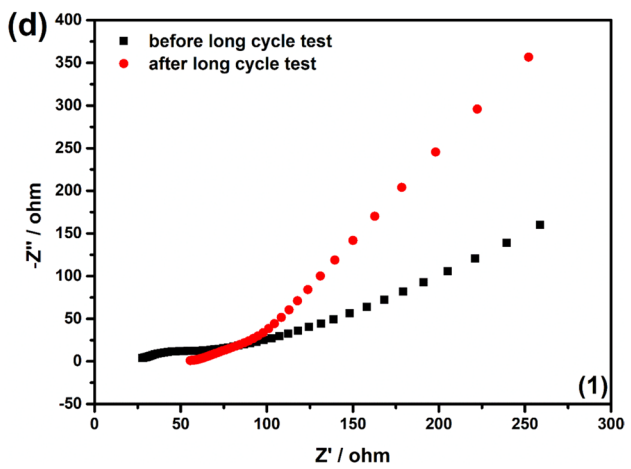


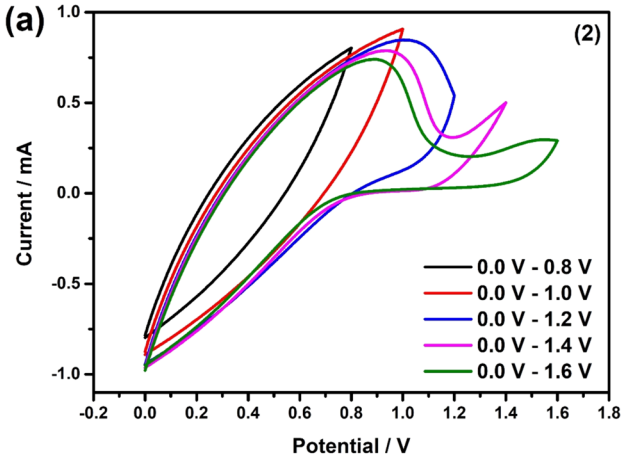


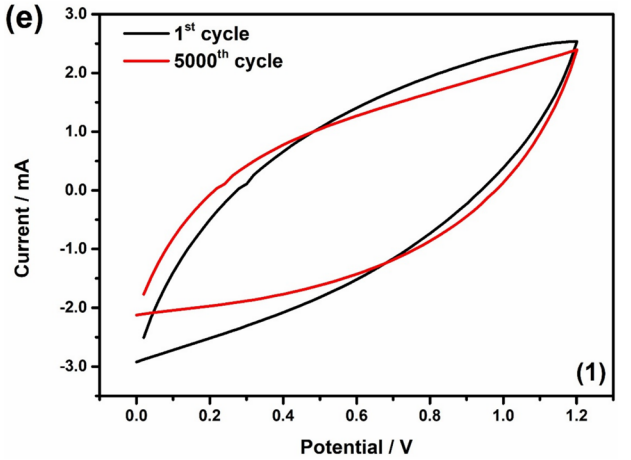


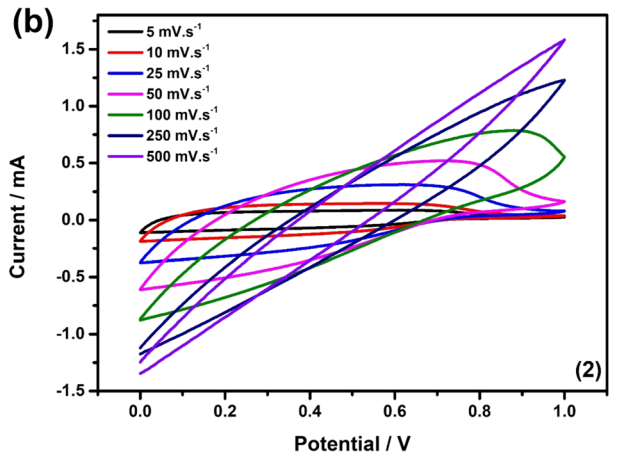


**Fig. 15** (continued)

## Electrochemical Performance of the Supercapacitor Device

The energy storage capacities of the PEDOT/PPy/(1)/PGE//PEDOT/PPy/(1)/PGE and PEDOT/PPy/(2)/PGE//PEDOT/PPy/(2)/PGE symmetric supercapacitors are shown in Figs. 15 and 16. A two-electrode electrochemical platform was employed to construct a symmetric supercapacitor, utilizing CV, GCD, and EIS measurements. PVA/0.5 M $H_2SO_4$ (10% w/w) gel electrolyte was used for the symmetric supercapacitor experiments. The measurements in Fig. 15a were taken in different potential windows. The supercapacitor showed the ability to store charges up to 1.2 V. However, given its exhibited resistance after 1.2 V during the charging and discharging cycles, the optimum operational range was determined to be between 0 V and +1.2 V. For the device performance test, cyclic voltammograms were recorded at scan rates of 5, 10, 25, 50, 100, 250, and 500 mV/s. The widening of the CV regions with increasing scan rate indicated that the reactions occurring on the electrode surface

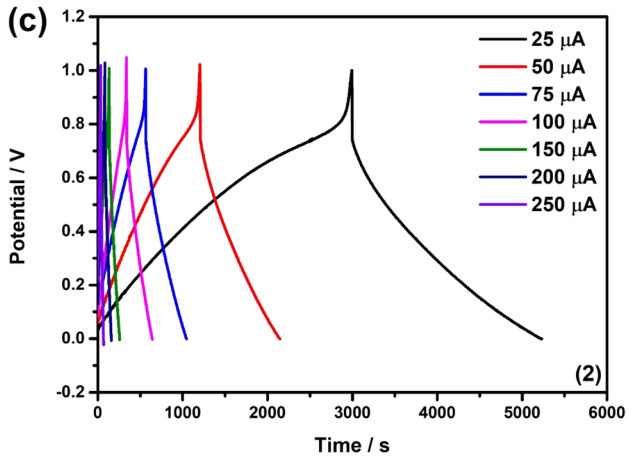


**Fig. 16** PEDOT/PPy/(2)/PGE//PEDOT/PPy/(2)/PGE symmetric supercapacitor in PVA/0.5 M $H_2SO_4$ (10% w/w) electrolyte; (a) CVs recorded in the range of 0.0–0.8 V, 0.0–1.0 V, 0.0–1.2 V, 0.0–1.4 V, and 0.0–1.6 V at a scan rate of 100 mV $s^{-1}$, (b) CVs recorded between 0.0 V and 1.0 V at different scan rates (5, 10, 25, 50, 100, 250, and 500 mV/s); (c) GCD curves recorded between 0.0 V and 1.0 V at different current values; (d) EIS Nyquist curves of before and after long-cycle tests; (e) long-cycle test for 5000 cycles.

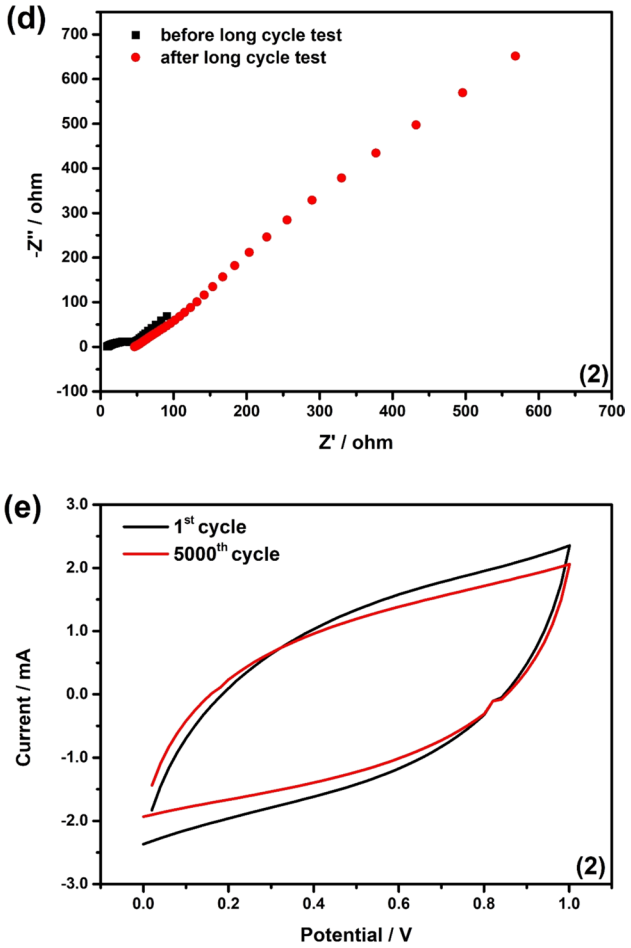


**Fig. 16** (continued)

were diffusion-controlled. The specific capacitance values in Fig. 15b were calculated as 29.6 ± 3.2, 18.4 ± 1.9, 13.4 ± 1.7, 12.6 ± 0.9, 7.7 ± 0.8, 5.4 ± 0.6, and 3.2 ± 0.6 F/g at scan rates of 5, 10, 25, 50, 100, 250, and 500 mV/s, respectively. The highest value of specific capacitance was obtained at a scan rate of 5 mV/s, with a result of 29.6 F/g. Furthermore, the fact that the cycle shapes did not change with increasing scan rate indicates that the electrode behaves stably. The specific capacitance values obtained for the PEDOT/PPy/(2)/PGE// PEDOT/PPy/(2)/PGE symmetric supercapacitor at different scan rates (5, 10, 25, 50, 100, 250, and 500 mV/s) shown in Fig. 16b were calculated as 61.8 ± 7.1, 47.1 ± 3.9, 33.7 ± 3.5, 29.6 ± 3.0, 19.6 ± 0.9, 9.8 ± 0.7, and 5.3 ± 0.4 F/g, respectively. The highest specific capacitance value was calculated as 61.8 F/g at a scan rate of 5 mV/s. The specific capacitance values obtained from the GCD curves of the PEDOT/PPy/(1)/PGE//PEDOT/PPy/(1)/PGE symmetric supercapacitor recorded at different currents were calculated as 18.2 ± 1.8, 16.7 ± 1.6, 15.4 ± 1.2, 15.2 ± 1.3, 13.4 ± 0.9, 9.9 ± 0.6, and 6.2 ± 0.4 F/g, respectively. The specific capacitance values obtained from the GCD curves of the PEDOT/PPy/(2)/PGE//PEDOT/PPy/(2)/PGE symmetric supercapacitor recorded at different currents were calculated as 53.4 ± 4.7, 41.0 ± 4.0, 34.6 ± 3.3, 29.5 ± 2.8, 17.6 ± 2.2, 13.0 ± 1.9, and 8.1 ± 0.7 F/g, respectively. The energy density ($E$) values of the PEDOT/PPy/(1)/PGE//PEDOT/PPy/(1)/PGE symmetric supercapacitor at different currents were calculated as 1.8, 1.7, 1.5, 1.5, 1.3, 1.0, and 0.6 Wh/kg, respectively. In addition, the power density ($P$) values were found as 6.5, 13.0, 19.6, 26.1, 39.1, 52.2, and 65.2 W/kg, respectively. The energy density ($E$) values of the PEDOT/PPy/(2)/PGE// PEDOT/PPy/(2)/PGE symmetric supercapacitor at different currents were calculated as 3.7, 2.8, 2.4, 2.1, 1.2, 0.9, and 0.6 Wh/kg, respectively. In addition, the power density ($P$) values were calculated as 6.0, 11.9, 17.9, 23.8, 35.7, 47.6, and 59.5 W/kg, respectively. The long-term cycling stability of the symmetric supercapacitor devices based on PEDOT/PPy/(1)/PGE and PEDOT/PPy/(2)/PGE electrodes was evaluated by cyclic voltammetry over 5000 continuous cycles at 100 mV $s^{-1}$ in a PVA/$H_2SO_4$ (10% w/w) gel electrolyte, as shown in Figs. 15e and 16e, respectively. In Fig. 15e, the PEDOT/PPy/(1)/PGE-based device maintained approximately 95.2% of its initial capacitance after 5000 cycles. The overlap between the first and last CV curves demonstrates minimal change in area, indicating high electrochemical stability and limited degradation of the polymer matrix and interface over repeated cycling. In Fig. 16e, the PEDOT/PPy/(2)/PGE-based supercapacitor retained approximately 97.6% of its initial capacitance after 5000 cycles. The nearly perfect overlap of the CV curves before and after cycling confirms outstanding stability, which is attributed to the enhanced morphological integrity, better $\pi$–$\pi$ conjugation, and more effective dopant–polymer interaction offered by compound **2**. These results highlight that both supercapacitor devices demonstrate excellent retention of electrochemical performance over prolonged cycling, with PEDOT/PPy/(2)/PGE achieving slightly superior stability. The minimal

**Table VII** Comparison of electrochemical impedance parameters before and after 5000 CV cycles for the PEDOT/PPy/(1)/PGE// PEDOT/PPy/(1)/PGE symmetric supercapacitor

| (1) | $R_s$ (Ω) | $C_{dl}$ (F) | $R_{ct}$ (Ω) | $W$ |
|---|---|---|---|---|
| Before | 27.793 | 3.9296E−6 | 58.566 | 0.00525 |
| After | 55.59 | 1090E−3 | 89.50 | 4015E−3 |

**Table VIII** Comparison of electrochemical impedance parameters before and after 5000 CV cycles for the PEDOT/PPy/(2)/PGE// PEDOT/PPy/(2)/PGE symmetric supercapacitor

| (2) | $R_s$ (Ω) | $C_{dl}$ (F) | $R_{ct}$ (Ω) | $W$ (Ω $s^{-1/2}$) |
|---|---|---|---|---|
| Before | 9.148 | 5.9673E−5 | 34.623 | 0.018395 |
| After | 46.57 | 251.2E−6 | 101.9 | 1.903E−3 |

loss in capacitance underscores the potential of these materials, particularly compound **2**-based systems, for practical applications requiring long-term durability.

The electrochemical stability of the symmetric supercapacitor devices fabricated with the PEDOT/PPy/(1)/PGE and PEDOT/PPy/(2)/PGE electrodes was evaluated by comparing their impedance parameters before and after long-term cycling, as presented in Tables VII and VIII. In the case of the PEDOT/PPy/(1)//PEDOT/PPy/(1) device (Table VII), a considerable increase was observed in both the series resistance ($R_s$) and charge transfer resistance ($R_{ct}$), from 27.8 Ω to 55.6 Ω and from 58.6 Ω to 89.5 Ω, respectively. These changes indicate a significant deterioration in the electrical conductivity and interfacial charge transfer efficiency, likely due to structural degradation of the electrode material over repeated cycling. Although the double-layer capacitance ($C_{dl}$) appeared to increase, this may be attributed to measurement artifacts caused by parasitic effects rather than an actual improvement in electrochemical performance. The decrease in Warburg impedance ($W$) also suggests hindered ion diffusion through the electrode matrix.

The PEDOT/PPy/(2)//PEDOT/PPy/(2) supercapacitor exhibited a more favorable stability profile (Table VIII). Although $R_s$ and $R_{ct}$ values also increased—from 9.1 Ω to 46.6 Ω and from 34.6 Ω to 101.9 Ω, respectively—the initial values were substantially lower, indicating better intrinsic conductivity and charge transfer kinetics at the beginning of the cycling test. Despite a reduction in Warburg impedance from 0.018 to 0.0019 Ω $s^{-1/2}$, which points to a moderate decrease in ion transport capability, the PEDOT/PPy/(2) electrode retained superior electrochemical characteristics. This relatively stable behavior is attributed to the improved structural integrity, more homogeneous dopant distribution, and enhanced $\pi$–$\pi$ interactions promoted by the pyrimidine-*N*-glycoside derivative (**2**).

The PEDOT/PPy/(2)/PGE electrode demonstrated outstanding maximum energy density of 45.8 Wh/kg at power density of 77.4 W/kg, which gradually decreased to 24.4 Wh/kg as the power density increased to 619.0 W/kg. This trend reflects the expected behavior of pseudocapacitive systems, where energy storage diminishes with higher discharge rates due to kinetic limitations. @@ Nonetheless, the retention of high energy at moderate-to-high power outputs illustrates the efficient ion/electron transport and stable redox activity enabled by the pyrimidine-*N*-glycoside (**2**) dopant. Li et al. synthesized a PEDOT/reduced graphene oxide (rGO) composite that achieved 22.5 Wh/kg at 320 W/kg, highlighting excellent rate capability but relatively moderate energy retention. Chen et al. developed a PPy/$MnO_2$ on carbon cloth electrode delivering 35.0 Wh/kg at 450 W/kg, suggesting strong pseudocapacitive behavior and good conductivity. Compared to these systems, the PEDOT/PPy/(2)/PGE electrode not only surpasses the reported materials in terms of maximum energy density, but also maintains a competitive power density range, confirming the advantageous synergy between the PEDOT-PPy copolymer backbone and the pyrimidine-*N*-glycoside (**2**) dopant. The combination of high energy storage, fast charge/discharge ability, and excellent electrochemical stability positions this material as a strong candidate for next-generation supercapacitor applications.

## Conclusions

In this study, novel composite electrodes PEDOT/PPy/(1)/PGE and PEDOT/PPy/(2)/PGE were successfully synthesized via electrochemical copolymerization in the presence of pyrimidine-*N*-glycoside derivatives (**1**) and (**2**), respectively. Among the investigated configurations, PEDOT/PPy/(2)/PGE demonstrated outstanding electrochemical performance, with specific capacitance of 195.2 F/g at 250 µA, along with energy density of 45.8 Wh/kg and power density of 77.4 W/kg. This performance is superior to that of the PEDOT/PPy/(1)/PGE electrode, which exhibited maximum specific capacitance of 97.4 F/g under similar conditions. In symmetric supercapacitor device configuration, the PEDOT/PPy/(2)/PGE//PEDOT/PPy/(2)/PGE system outperformed its counterpart, achieving maximum specific capacitance of 61.8 F/g at 5 mV/s, with corresponding energy density of 3.7 Wh/kg and power density of 59.5 W/kg. The device also maintained high stability, with minimal capacitance degradation after prolonged cycling. These results indicate that the integration of pyrimidin-*N*-glycoside derivative (**2**) enhances the electrochemical activity and morphological characteristics of the conducting polymer matrix, particularly through improved $\pi$–$\pi$ interactions and optimized dopant distribution, as supported by XRD, Raman, FTIR, and SEM analyses.

**Author Contributions** All authors contributed to the study conception and design. Material preparation and data collection were performed by Nilufer Kocyigit, Fatma Demir, Özlem Yağci, Melih Besir Arvas and Nuran Kahriman. Analysis were performed by Nilufer Kocyigit, Fatma Demir, Özlem Yağci, Melih Besir Arvas and Nuran Kahriman. The first draft of the manuscript was written by Nilufer Kocyigit, Fatma Demir, Özlem Yağci, Melih Besir Arvas and Nuran Kahriman, and all authors commented on previous versions of the manuscript. All authors read and approved the final manuscript.

**Funding** Open access funding provided by the Scientific and Technological Research Council of Türkiye (TÜBİTAK). The authors received no financial support for the research, authorship, and/or publication of this article.

**Data Availability** The datasets generated and/or analyzed during the current study are available from the corresponding author on reasonable request.

**Conflict of interest** The authors declare that they have no known competing financial interests or personal relationships that could have appeared to influence the work reported in this paper.

**Open Access** This article is licensed under a Creative Commons Attribution 4.0 International License, which permits use, sharing, adaptation, distribution and reproduction in any medium or format, as long as you give appropriate credit to the original author(s) and the source, provide a link to the Creative Commons licence, and indicate if changes were made. The images or other third party material in this article are included in the article's Creative Commons licence, unless indicated otherwise in a credit line to the material. If material is not included in the article's Creative Commons licence and your intended use is not permitted by statutory regulation or exceeds the permitted use, you will need to obtain permission directly from the copyright holder. To view a copy of this licence, visit http://creativecommons.org/licenses/by/4.0/.

## References

1. H.W. Park and K.C. Roh, *J. Power. Sources* 557, 232558 (2023).
2. D. Maradin, *Int. J. Energy Econ. Policy* 11, 176 (2021).
3. S. Gümrükçü, E. Kaplan, M.B. Arvas, N. Koçyiğit, M. Özçeşmeci, Y. Şahin, and İ Özçeşmeci, *Energy Technol.* 13, 2400915 (2025).
4. J. Mitali, S. Dhinakaran, and A.A. Mohamad, *Energy Storage Sav.* 1, 166 (2022).
5. A.G. Olabi and M.A. Abdelkareem, *Energy* 219, 119634 (2021).
6. M.S. Shalaby, M.O. Alziyadi, H. Gamal, and S. Hamdy, *J. Alloys Compd.* 969, 172318 (2023).
7. N.N. Loganathan, V. Perumal, B.R. Pandian, R. Atchudan, T.N.J.I. Edison, and M.J. Ovinis, *Energy Storage* 49, 104149 (2022).
8. N. Koçyiğit, A.T.A. Ramzy, S. Yazar, M.B. Arvas, N. Acar-Selçuki, M. Özer, and Ö. Bekaroğlu, *ECS J. Solid State Sci. Technol.* 13, 113004 (2024).
9. L. Zhang, X. Hu, Z. Wang, F. Sun, and D.G. Dorrell, *Renew. Sustain. Energy Rev.* 81, 1868 (2018).
10. F. Naseri, S. Karimi, E. Farjah, and E. Schaltz, *Renew. Sustain. Energy Rev.* 155, 111913 (2022).
11. N. Choudhary, C. Li, J. Moore, N. Nagaiah, L. Zhai, Y. Jung, and J. Thomas, *Adv. Mater.* 29, 1605336 (2017).
12. M.B. Arvas, H. Gürsu, M. Gençten, and Y.J. Şahin, *Energy Storage* 35, 102328 (2021).
13. N. Koçyiğit, M.B. Arvas, S. Yazar, N. Açar-Selçuki, Y. Şahin, M. Özer, and Ö. Bekaroğlu, *Synth. Met.* 292, 117242 (2023).
14. M. Pershaanaa, S. Bashir, S. Ramesh, and K.J. Ramesh, *Energy Storage* 50, 104599 (2022).
15. N. Kumar, S.B. Kim, S.Y. Lee, and S.J. Park, *Nanomaterials* 12, 3708 (2022).
16. A.V. Hacinecipoglu and M. Gençten, *FlatChem* 49, 100800 (2025).
17. A.M. Elshahawy, S.M. Elkatlawy, M.S. Shalaby, C. Guan, and J. Wang, *J. Electron. Mater.* 52, 1347 (2022).
18. S. Karthikeyan, B. Narenthiran, A. Sivanantham, L.D. Bhatlu, and T. Maridurai, *Mater. Today Proc.* 46, 3984 (2021).
19. H. Gamal, A.M. Elshahawy, S.S. Medany, M.A. Hefnawy, and M.S.J. Shalaby, *Energy Storage* 76, 109788 (2024).
20. L. Cheng, S. Kakita, R. Fox, N.I. Jalal, R.I. Ibrahim, and M.K. Oudah, *J. Phys. Conf. Ser.* 1973, 012015 (2021).
21. M.E. Şahin, F. Blaabjerg, and A. Sangwongwanich, *Energies* 15, 674 (2022).
22. M. Conte, *Fuel Cells* 10, 806 (2010).
23. N. Kocyigit, S.D. Zor, O. Yagci, S.B. Uzuncam, and M.B. Arvas, *Synth. Met* 311, 117795 (2025).
24. N. Kocyigit, M. Gencten, M. Sahin, and Y. Sahin, *Int. J. Energy Res.* 45, 6850 (2021).
25. S. Gümrükçü, M. Özçeşmeci, N. Koçyiğit, K. Kaya, A. Gül, Y. Şahin, and İ Özçeşmeci, *Dalton Trans.* 52, 13164 (2023).
26. N. Kocyigit, S.D. Zor, O. Yagci, and M.B. Arvas, *J. Mater. Sci. Mater. Electron.* 35, 2196 (2024).
27. A. Ranjbar Aghjehkohal, A. Taghizadeh Tabrizi, and M. Yildiz, *J. Alloys Compd.* 935, 168083 (2023).
28. Z. Chen, E. Villani, and S. Inagi, *Curr. Opin. Electrochem.* 28, 100726 (2021).
29. S. Lin, Q. Wu, and Y. Lu, *ChemElectroChem* 11, e202400073 (2024).
30. P. Keerthana, A. George, L. Benny, and A. Varghese, *Electrochim. Acta* 445, 142071 (2023).
31. A. Moyseowicz, D. Minta, and G. Gryglewicz, *ChemElectroChem* 10, e202300228 (2023).
32. N. Kocyigit, S. Dinc-Zor, O. Yagci, and M.B. Arvas, *J. Mater. Res.* 40, 1 (2025).
33. N. Kahriman, K. Peker, V. Serdaroğlu, A. Aydın, B. Türkmenoğlu, A. Usta, and N. Yaylı, *Turk. J. Chem.* 47, 476 (2023).
34. N. Kahriman, V. Serdaroğlu, A. Aydın, B. Türkmenoğlu, and A. Usta, *J. Mol. Struct.* 1277, 134821 (2023).
35. M. Dashti Najafi, E. Kowsari, H.R. Naderi, S. Sarabadani Tafreshi, A. Chinnappan, S. Ramakrishna, N.H. de Leeuw, and A. Ehsani, *J. Mol. Liq.* 348, 118381 (2022).
36. T. Tooming, T. Thomberg, H. Kurig, A. Jänes, and E. Lust, *J. Power. Sources* 280, 667 (2015).
37. N. Kahriman, V. Serdaroğlu, K. Peker, A. Aydın, A. Usta, S. Fandaklı, and N. Yaylı, *Bioorg. Chem.* 83, 580 (2019).
38. N. Kahriman, K. Peker, V. Serdaroğlu, A. Aydın, A. Usta, S. Fandaklı, and N. Yaylı, *Bioorg. Chem.* 99, 103805 (2020).
39. E. Hosseini, V. Ozhukil Kollath, and K. Karan, *J. Mater. Chem. C* 8, 3982 (2020).
40. S. Krishnaswamy, V. Ragupathi, S. Raman, P. Panigrahi, and G.S. Nagarajan, *Polym. Bull.* 76, 5213 (2019).
41. W. Shi, T. Zhao, J. Xi, D. Wang, and Z. Shuai, *J. Am. Chem. Soc.* 137, 12929 (2015).
42. Ö. Yağci, *Physica B* 686, 416089 (2024).
43. M.B. Arvas, S. Yaylagül, K. Uzbiçen, N. Koçyiğit, and Ö. Yağci, *J. Alloys Compd.* 1016, 178879 (2025).
44. S. Munusamy, R. Suresh, K. Giribabu, R. Manigandan, S. Praveen Kumar, S. Muthamizh, C. Bagavath, A. Stephen, J. Kumar, and V. Narayanan, *Arab. J. Chem.* 12, 3565 (2019).
45. S. Radhakrishnan, C. Sumathi, A. Umar, S.J. Kim, J. Wilson, and V. Dharuman, *Biosens. Bioelectron.* 47, 133 (2013).
46. X. Hu, G. Chen, X. Wang, and H.J. Wang, *Mater. Chem. A* 3, 20896 (2015).
47. Khan S, Alkhedhe M, Raza R, Ahmad MA, Majid A, and Tag El Din EM. (2022), Polymers, 14, 1976.
48. H. Zhu, M. Li, D. Wang, S. Zhou, and C. Peng, *J. Electrochem. Soc.* 164, A1820 (2017).

**Publisher's Note** Springer Nature remains neutral with regard to jurisdictional claims in published maps and institutional affiliations.